Effect of spin-phonon interaction on the Raman spectra of quasi-two-dimensional Heisenberg antiferromagnets

Dirk Uwe Saenger*
Institut für Theoretische Physik, Universität des Saarlandes, 66041 Saarbrücken, Germany
(Received 7 February 1995)

Using the Dyson-Maleev representation of the spin opertors, the two-magnon Raman spectra (B_{1g} geometry) in quasi-two-dimensional Heisenberg antiferromagnets at finite temperatures are calculated. The two-magnon spectrum is computed in a self-consistent manner within the framework of a renormalized harmonic approximation, which is correct up to order $1/S$ in the $1/S$ expansion of perturbation theory. Including a renormalization of the one-magnon spectral function due to the intrinsic spin part of the model up to order $1/S^2$ and due to spin-phonon interaction up to order $1/S$, it is shown that spin-phonon interaction generates a significant broadening of the one-magnon spectral function at the Brillouin-zone boundary in the regime where sound velocities are small compared to magnon velocities. In that regime it dominates the spectral feature of the two-magnon Raman line. Based on that result, the anomalous broadening of the two-magnon spectrum, observed in light-scattering experiments on antiferromagnets with large maximum magnon energies such as, e.g., the spin-$\frac{1}{2}$ compound La_2CuO_4 and the spin-1 compound Pr_2NiO_4, can be described mainly as a consequence of spin-phonon interaction. This effect is absent in systems with smaller exchange integrals such as, e.g., La_2NiO_4 or K_2NiF_4, respectively. Accordingly, it is safe to postulate that the broad spectral feature observed experimentally is generated by spin-phonon interaction. In order to explain the line shape in the cuprates completely, especially the high-energy tail, four-magnon contributions due to nearest-neighbors spin-pair excitations and higher contributions in the effective Raman-scattering Hamiltonian due to the resonant enhancement of the Raman cross section have to be considered and will be discussed on a qualitative basis.

I. INTRODUCTION

Light-scattering experiments on quasi-two-dimensional (2D) antiferromagnets with spin $S \geq \frac{1}{2}$ have attracted a lot of interest in the last two decades, especially since the discovery of superconductivity in doped 2D antiferromagnets such as La_2CuO_4. Here we will be concerned with the question of the large broadening of the B_{1g} Raman line involving spin-pair excitations on neighboring sites, which make the highest contribution to the whole B_{1g} Raman cross section, observed in Raman-scattering experiments in undoped high-T_c superconductor basic materials with spin-$\frac{1}{2}$ such as La_2CuO_4 and the nickelate Pr_2NiO_4 with spin-1. The important issue from the theoretical side consists in a consistent microscopic interpretation of the B_{1g} Raman line shape. The latter is produced by two- and four-magnon processes and the problem addressed in this paper refers to the origin of the spectral broadening and anomalous line shape being of intrinsic (magnonlike) or extrinsic (phononic) origin. Based on an extension to the third dimension of a recently developed theory, we provide theoretical evidence, that spin-phonon interaction causes the anomalous spectral feature in layered compounds with large maximum magnon energies. In order to put the problem into proper reference some important experimental and theoretical developments in the field of light scattering will be reviewed first.

At the end of the sixties and the early seventies Raman-scattering experiments[1] were performed in spin-1 antiferromagnets such as K_2NiF_4. The observed B_{1g} Raman spectrum (for a recent derivation of the effective Raman-scattering Hamiltonian in the framework of a one-band Hubbard model, see Shastry and Shraiman[2]) could be well described within the framework of an intrinsic spin-wave model,[3,4] using the Raman-scattering Hamiltonian derived by Fleury and Loudon[5] and Elliott and Thorpe,[6] respectively, which contains only spin-pair excitations on neighboring sites. These authors computed the two-magnon spectrum and included magnon-magnon interaction at the level of a renormalized harmonic approximation (RHA) or ladder approximation, respectively.[4] That means the one-magnon and two-magnon states are renormalized in a self-consistent way up to order $1/S$ in perturbation theory. Due to the attraction between the two magnons the Raman spectrum has its maximum at an energy smaller than twice the maximum magnon energy. Four-magnon production by light was neglected completely, because that spectrum was assumed to be well separated from the two-magnon spectrum and to have a very small spectral weight compared to the two-magnon spectrum in the case of spin-1.

At the end of the eighties and the beginning nineties the same experiments were done in spin-1/2 systems such as the one-layer systems $(La,Sm,Nd,Pr)_2CuO_4$ (Refs. 7–10) and the two-layer system $YBa_2Cu_3O_6$,[9,11–12] usually called cuprates, and the spin-1 systems such as the one-layer systems $(Pr,La)_2NiO_4$,[9,13] usually called nickelates. The experiments in the cuprates with in-plane exchange integrals of order 90–130 meV, yielding max-

imum magnon energies of 200–300 meV ($S=\frac{1}{2}$) and the nickelate Pr_2NiO_4 with an exchange integral of 50 meV and a maximum magnon energy of 200 meV ($S=1$), showed a broad spectral feature. In the cuprates these spectra extend to a long energy tail, which can not be described in RHA, neglecting four-magnon contributions, because there does not exist a finite Raman cross section above twice the maximum magnon energy.

Accordingly, Singh *et al.*[7] predicted that the intrinsic properties of the spin-$\frac{1}{2}$ system, i.e., quantum fluctuations, should produce such a spectral feature, although neutron-scattering experiments[14–18] and theoretical calculations[19–23] showed that a renormalized spin-wave model describes all the other experimental and theoretically calculated data, which were obtained for instance by Monte Carlo simulations (for a review, see, Ref. 24), very well. They supported this suggestion with the calculation of the first three frequency moments of the B_{1g} mode within the framework of the Fleury-Loudon-Elliott-Thorpe Hamiltonian, which define the mean value of the frequency, the fluctuations and the asymmetry of the spectrum, using series expansions around the Ising limit. These frequency moments were in rather good agreement with the measured ones, but as pointed out by Canali and Girvin[25] they can not resolve the line shape of the Raman spectrum. Thus a microscopic theory of the line shape is still lacking. Nevertheless, the calculations of Singh *et al.*[7] show, that four-magnon production by the light-scattering process cannot be neglected deliberately. As a result, Canali and Girvin[25] performed calculations of the Raman spectrum, using the same scattering Hamiltonian, in the framework of an intrinsic spin-wave model in order to obtain a microscopic picture of the line shape of the Raman spectrum, including four-magnon contributions and renormalization effects of the one-magnon spectral function up to order $1/S^2$. Their motivation was to check the possibility if the high-energy tail in the Raman spectra, which is the key point to understand the spectral feature, is generated by high-energy excitations involving four magnons and the renormalization of the one-particle spectrum. They showed, however, that the spectral feature obtained was in poor agreement with the measured one, because the $1/S^2$ contributions turned out to be small and fail to broaden the Raman line in a significant manner. The calculations of the four-magnon spectrum (called direct four-magnon production in Ref. 25) by Canali and Girvin[25] were not done self-consistently. A possible consequence of that was a too high predicted peak position of the four-magnon peak. In a further attempt they estimated the peak position of the four-magnon spectrum and obtained a peak position at $5\times J_{\text{eff}}$ and an intensity of approximately 10% of the two-magnon spectrum. However, due to the narrow two-magnon and four-magnon spectrum, the peaks were well separated and the observed Raman spectrum was still in poor agreement with the measured one.

De Andrés, Martinez, and Odier[13] performed light-scattering experiments on the spin-1 2D antiferromagnet Pr_2NiO_4 with an effective in-plane exchange integral of approximately 50 meV, yielding a maximum magnon energy of 200 meV, and observed a similar spectral feature as in the cuprates. This suggests that the anomalous spectral feature is not generated completely by the intrinsic nature of a spin-$\frac{1}{2}$ system. Sugai *et al.*[9] measured the two-magnon line in the spin-1 system La_2NiO_4 with an effective exchange of 30 meV, giving a maximum magnon energy of 120 meV, and showed, that this nickelate does not have such a broad spectral feature as the cuprates and the nickelate Pr_2NiO_4. In order to explain the high-energy tail in the cuprates Sugai *et al.*[9] suggested, that a four-spin cyclic interaction, derived via an extended Hubbard model, should produce at least partially the high-energy tail via the production of four magnons. As a result, the magnon dispersion should be altered as compared to the Heisenberg model, but neutron-scattering experiments[14–16] show that the Heisenberg model describes the dispersion of the magnons very well and we may neglect such an interaction.

Furthermore, Knoll *et al.*[11] measured the temperature-dependent spectral feature in $YBa_2Cu_3O_6$ and showed, that the linewidth of the two-magnon line is strongly temperature dependent [the peak intensity at room temperature is approximately 25% smaller than at low temperatures in $YBa_2Cu_3O_6$ and approximately 10% smaller in the one-layer systems such as La_2CuO_4 (Ref. 9)], which would not be the case, if we consider only an intrinsic spin model, because of the high-energy excitations (>100 meV) involved in the scattering process. They concluded, that the anomalous spectral feature and its temperature dependence is generated by low-energy phonon excitations, because of a possible spontaneous decay process in antiferromagnets, where a magnon decays into another magnon and a phonon under the condition that the sound velocities are smaller than the magnon velocities. In a recent contribution[26] we calculated the damping of spin waves in the limit $k\xi \gg 1$ (ξ is the correlation length of the 2D system) due to the compressibility of a square lattice. We showed that the temperature-dependent linewidth of the two-magnon Raman line in the two-layer system $YBa_2Cu_3O_6$, measured by Knoll *et al.*,[11] could be described qualitatively by the broadening of the one-magnon spectral function at the 2D Brillouin-zone boundary (BZB), where the highest contribution to the damping is generated by spin-phonon interaction.

In this paper we extend calculations of the one-magnon spectral function in one-layer systems such as La_2CuO_4 in the short-wavelength regime, by taking account of the third spatial dimension of the problem, which was ignored in Ref. 26. Furthermore, we generalize the theories of the two-magnon Raman spectrum of Davies, Chinn, and Zeiger[4] and Canali and Girvin[25] taking account of spin-phonon interaction. As a result we can show that the measured two-magnon spectrum in the cuprates is in good agreement with the calculated two-magnon cross section. Furthermore, it is shown that the spontaneous decay process, which produces the damping of magnons, is only effective in systems with large maximum magnon energies, yielding large magnon velocities. Accordingly, the spectral feature in the spin-1 systems La_2NiO_4 and K_2NiF_4 has to be smaller. The kink and the high-energy tail in the Raman spectrum, see, e.g.,

Fig. 8 below, in the measurements of Sugai *et al.*[9] and Singh *et al.*,[7] can now be explained as generated by the four-magnon contributions of the nearest-neighbor spin-pair excitations and higher contributions in the effective Raman-scattering Hamiltonian due to the resonant enhancement of the Raman cross section via the resonant excitation of transitions close to the charge-transfer gap,[2] i.e., higher contributions in the $t/(U-\hbar\omega_i)$ expansion have to be considered, where t and U are the hopping and the repulsion term of the effective one-band Hubbard model, respectively. ω_i is the frequency of the incident light.[27] The four-magnon contributions due to spin-pair excitations on neighboring sites (assuming that this term makes the highest contribution to the high-energy tail of the Raman cross section B_{1g} mode) have to be calculated in a self-consistent manner, i.e., repeated ladder interactions between the four magnons has to be considered and the broadening of the one-magnon spectral function due to spin-phonon interaction has to be taken into account. That is, of course, a heavy work as was already pointed out by Canali and Girvin.[25] Here we do not execute such calculations here, but discuss such effects on a qualitative basis.

The paper is organized as follows. In Sec. II the model studied will be explained, the transformation to Boson operators is introduced and the spin-wave spectrum is calculated in renormalized harmonic approximation, i.e., $1/S$ contributions are considered. In Sec. III the self-energy of magnons in Born approximation (BA) is calculated. Using the results of Sec. III, the two-magnon Raman cross section is calculated in Sec. IV and the results are compared with the measured Raman spectra. In Sec. V some conclusions are drawn.

II. FORMALISM

A. Model

The model that we study is given by the effective Hamiltonian $H=H^S+H^{\mathrm{SP}}+H^P$, where the spin ($H^S$) and the spin-phonon ($H^{\mathrm{SP}}$) Hamiltonian in harmonic approximation are defined by

$$H^S+H^{\mathrm{SP}}=\sum_{\langle l,l'_{\parallel}\rangle}[1+(\mathbf{u}_l-\mathbf{u}_{l'_{\parallel}})\cdot\nabla]J(|\mathbf{R}_l-\mathbf{R}_{l'_{\parallel}}|)\mathbf{S}_l\cdot\mathbf{S}_{l'_{\parallel}}+\sum_{\langle l,l'_{\perp}\rangle}[1+(\mathbf{u}_l-\mathbf{u}_{l'_{\perp}})\cdot\nabla]J(|\mathbf{R}_l-\mathbf{R}_{l'_{\perp}}|)\mathbf{S}_l\cdot\mathbf{S}_{l'_{\perp}}. \tag{1}$$

The sums run over the nearest neighbors on a tetragonal lattice, where the spins form a Néel-like configuration and l and $l'_{\parallel},l'_{\perp}$ refer to the sites of spin-up (A) and spin-down (B) Néel sublattices, respectively, with the subindices referring to in-plane and out-of-plane couplings. For nearest neighbors we may set

$$\begin{aligned}
&J(|\mathbf{R}_l-\mathbf{R}_{l'_{\parallel}}|)=J,\\
&\nabla\cdot\mathbf{J}(|\mathbf{R}_l-\mathbf{R}_{l'_{\parallel}}|)=-|\nabla\mathbf{J}(a)|\frac{\mathbf{R}_l-\mathbf{R}_{l'_{\parallel}}}{|\mathbf{R}_l-\mathbf{R}_{l'_{\parallel}}|},\\
&J(|\mathbf{R}_l-\mathbf{R}_{l'_{\perp}}|)=\alpha_{\perp}J,\\
&\nabla\cdot J(|\mathbf{R}_l-\mathbf{R}_{l'_{\perp}}|)=-\alpha_{\perp}|\nabla J(a)|\frac{\mathbf{R}_l-\mathbf{R}_{l'_{\perp}}}{|\mathbf{R}_l-\mathbf{R}_{l'_{\perp}}|},
\end{aligned} \tag{2}$$

where J is the in-plane exchange integral and the out-of-plane exchange integral $J_{\perp}$ scales with $\alpha_{\perp}$ in units of J, where $\alpha_{\perp}$ is very small in all the systems ($\alpha_{\perp}\leq 5\times 10^{-5}$) considered. Furthermore, we assumed, that the out-of-plane modulation integral scales also with $\alpha_{\perp}$ and because we are interested in short-wavelength excitations we neglect the small anisotropies. Neglecting the spin-phonon part of the Hamiltonian in (1), our Hamiltonian coincides with the effective Hamiltonian used by Keimer *et al.*[15] and Kopietz[22] in order to describe some magnetic properties of the cuprates. The in-plane and the out-of-plane lattice constants are represented by a and c, respectively. We measure in-plane and out-of-plane length in units of in-plane and out-of-plane lattice constants, respectively. $\mathbf{u}_l$ is the displacement operator and $\mathbf{S}$ is the dimensionless spin operator. The Hamiltonian for the lattice system is given by

$$H^p=\sum_{i,\alpha}\frac{p_{i,\alpha}^2}{2m}+\frac{1}{2}\sum_{\substack{i,i'\\ \alpha,\beta}}u_{i,\alpha}\phi_{\alpha,\beta}(|\mathbf{R}_i-\mathbf{R}_{i'}|)u_{i',\beta}, \tag{3}$$

where $\phi_{\alpha,\beta}|(\mathbf{R}_i-\mathbf{R}_{i'}|)$ are effective force constants and $\mathbf{p}_i$ is a momentum operator. The sums run over the whole lattice and the greek indices indicate Cartesian coordinates. We neglect the existence of high-energy optical phonons in the real systems, because the temperature dependence of the one-magnon spectral function is dominated by long-wavelength acoustic phonons. High-energy optical phonons can make only temperature-independent contributions to the renormalization of the magnons, because the Bose distribution functions for optical phonons are small in the temperature regime considered here, and are assumed to be smaller than the acoustic part, since most high-energy phonons contain only oxygen displacements, which do not modulate the Cu-Cu distance in our effective model and the spin-phonon coupling constants, to be defined later, are smaller for optical phonons ($\sim 1/\omega_{\mathrm{opt}}^{1/2}$). As a result, we assume that long-wavelengths acoustic phonons are the most important in the scattering processes.

Fourier transformation of (3) yields

$$H^p=\sum_{q,j}\hbar\omega_j(\mathbf{q})\left[c_j^{+}(\mathbf{q})c_j(\mathbf{q})+\frac{1}{2}\right], \tag{4}$$

where $c_j^{+}(\mathbf{q})$ and $c_j(\mathbf{q})$ are creation and annihilation operators for phonons of wave vectors $\mathbf{q}$ and phonon branch j, where j indicates transversally and longitudinally polarized acoustic phonons. The sum over the wave

vectors $\mathbf{q}$ runs over the Brillouin zone (BZ) of the mechanical lattice (BZ_p). Notice that we get the purely three-dimensional Hamiltonian of Ref. 31, if we set $\alpha_\perp$ equal to one and the purely 2D Hamiltonian of Ref. 26, if we set $\alpha_\perp$ equal to zero and neglect the mechanical coupling between the layers.

B. Bosonization of the Heisenberg Hamiltonian

Using the Dyson-Maleev transformation (DM),[32,33] which is given by

$$\begin{aligned} S_l^+ &= (2S)^{1/2}(1-a_l^+ a_l/2S)a_l \ , \\ S_l^- &= (2S)^{1/2}a_l^+ \ , \\ S_l^z &= S - a_l^+ a_l \ , \end{aligned} \tag{5}$$

for the A sublattice and

$$\begin{aligned} S_{l'}^+ &= (2S)^{1/2}b_{l'}^+(1-b_{l'}^+ b_{l'}/2S) \ , \\ S_{l'}^- &= (2S)^{1/2}b_{l'} \ , \\ S_{l'}^z &= -S + b_{l'}^+ b_{l'} \ , \end{aligned} \tag{6}$$

for the B sublattice, we may transform the Hamiltonian in (1) into a boson Hamiltonian. The Fourier transforms of the boson operators are given by

$$\begin{aligned} a_l &= \left[\frac{2}{N}\right]^{1/2} \sum_k e^{i\mathbf{k}\cdot\mathbf{R}_l} a_k \ , \\ b_{l'} &= \left[\frac{2}{N}\right]^{1/2} \sum_k e^{i\mathbf{k}\cdot\mathbf{R}_{l'}} b_k \ , \end{aligned} \tag{7}$$

and their Hermitian conjugates; $\mathbf{k}$ runs over the magnetic Brillouin zone (BZ_m) and N is the total number of atoms. Similarly, the Fourier transforms of the displacement operator is given by

$$\mathbf{u}_i = \sum_{q,j} \left[\frac{\hbar}{2Nm\omega_j(\mathbf{q})}\right]^{1/2} \mathbf{e}(\mathbf{q},j)e^{-i\mathbf{q}\cdot\mathbf{R}_i} \times [c_j^+(\mathbf{q}) + c_j(-\mathbf{q})] \ , \tag{8}$$

where $\mathbf{e}(\mathbf{q},j)$ represents the polarization vector for wave vector $\mathbf{q}$ and phonon branch j. Equations (7) and (8) inserted into H^S and H^{SP} yields, respectively,

$$\begin{aligned} H_{DM}^S = &-4(1+\alpha_\perp/2)JS^2N/2 + H_e \sum_k \gamma'(\mathbf{k})(a_k b_{-k} + a_k^+ b_{-k}^\pm) + (1+\alpha_\perp/2)(a_k^+ a_k + b_{-k}^\pm b_{-k}) \\ &- H_e/NS \sum_{k_1,k_2,k_3,k_4} \delta_G(\mathbf{k}_1+\mathbf{k}_2-\mathbf{k}_3-\mathbf{k}_4)[\gamma'(\mathbf{k}_2)a_{k_1}^+ b_{-k_2} a_{k_3} a_{k_4} + \gamma'(\mathbf{k}_2-\mathbf{k}_3-\mathbf{k}_4)a_{k_1}^+ b_{-k_3}^\pm b_{-k_4}^\pm b_{-k_2} \\ &+ 2\gamma'(\mathbf{k}_2-\mathbf{k}_4)a_{k_1}^+ a_{k_3} b_{-k_4}^\pm b_{-k_2}] \ , \end{aligned} \tag{9}$$

$$\begin{aligned} H^{SP} = &-iBH_e \sum_{k_1,k_2,q,j} \delta_G(\mathbf{k}_1-\mathbf{k}_2-\mathbf{q}) \left[\frac{\hbar}{2Nm\omega_j(\mathbf{q})}\right]^{1/2} \\ &\times \{[\Delta'(\mathbf{q},j,\mathbf{k}_2) - \Delta'(\mathbf{q},j,\mathbf{k}_2+\mathbf{q})]a_{k_1} b_{-k_2} - [\Delta'(\mathbf{q},j,\mathbf{k}_1) - \Delta'(\mathbf{q},j,\mathbf{k}_1+\mathbf{q})]a_{k_2}^+ b_{-k_1}^\pm \\ &- \Delta'(\mathbf{q},j,\mathbf{k}_1)a_{k_2}^+ a_{k_1} - \Delta'(\mathbf{q},j,\mathbf{k}_1+\mathbf{q})b_{-k_1}^\pm b_{-k_2}\} u_j(\mathbf{q}) \\ &- iBH_e/SN \sum_{k_1,k_2,k_3,k_4} \delta_G(\mathbf{k}_1+\mathbf{k}_2-\mathbf{k}_3-\mathbf{k}_4+\mathbf{q}) \left[\frac{\hbar}{2Nm\omega_j(\mathbf{q})}\right]^{1/2} \\ &\times \{-[\Delta'(\mathbf{q},j,\mathbf{k}_2) - \Delta'(\mathbf{q},j,\mathbf{k}_2+\mathbf{q})]a_{k_1}^+ b_{-k_2} a_{k_3} a_{k_4} \\ &+ [\Delta'(\mathbf{q},j,\mathbf{k}_3+\mathbf{k}_4-\mathbf{k}_2) - \Delta'(\mathbf{q},j,\mathbf{k}_3+\mathbf{k}_4-\mathbf{k}_2-\mathbf{q})]a_{k_1}^+ b_{-k_3}^\pm b_{-k_4}^\pm b_{-k_2} \\ &- 2[\Delta'(\mathbf{q},j,\mathbf{k}_2,-\mathbf{k}_4) - \Delta'(\mathbf{q},j,\mathbf{k}_2-\mathbf{k}_4+\mathbf{q})]a_{k_1}^+ b_{-k_4}^\pm a_{k_3} b_{-k_2}\} u_j(\mathbf{q}) \ . \end{aligned} \tag{10}$$

Here the Kronecker symbol implements the conservation of momentum with respect to umklapp processes, and $\mathbf{G}$ is a reciprocal-lattice vector of the magnetic lattice. In (9) and (10) the following abbreviations have been introduced:

$$H_e=4SJ,\quad B=4S|\nabla J(a)|/H_e\ ,$$

$$\gamma'(\mathbf{k})=\frac{1}{4}\left[\sum_{\delta_\parallel}e^{i\mathbf{k}\cdot\delta_\parallel}+\alpha_\perp\sum_{\delta_\perp}e^{i\mathbf{k}\cdot\delta_\perp}\right]=\gamma(\mathbf{k}_\parallel)+\frac{\alpha_\perp}{2}\cos(k_z)\ ,$$

$$\gamma(\mathbf{k}_\parallel)=\frac{1}{2}[\cos(k_x)+\cos(k_y)]\ ,$$

$$\begin{aligned}i\Delta'(\mathbf{q},j,\mathbf{k})&=-\frac{1}{4}\sum_{\delta_\parallel}\frac{\delta_\parallel}{|\delta_\parallel|}\mathbf{e}(\mathbf{q},j)e^{-i\mathbf{k}\cdot\delta_\parallel}-\frac{\alpha_\perp}{4}\sum_{\delta_\perp}\frac{\delta_\perp}{|\delta_\perp|}\mathbf{e}(\mathbf{q},j)e^{-i\mathbf{k}\cdot\delta_\perp}\\&=i\frac{1}{2}\sum_{\alpha=x,y}e_\alpha(\mathbf{q},j)\sin(k_\alpha)+i\frac{\alpha_\perp}{2}e_z(\mathbf{q},j)\sin(k_z)\\&=i\Delta(\mathbf{q},j,\mathbf{k}_\parallel)+i\frac{\alpha_\perp}{2}e_z(\mathbf{q},j)\sin(k_z)\ ,\end{aligned}\tag{11}$$

$$u_j(\mathbf{q})=c_j^+(\mathbf{q})+c_j(-\mathbf{q})\ ,$$

where the sums run over the nearest neighbors of a tetragonal lattice. Note that we divided the function $\Delta'(\mathbf{q},j,\mathbf{k})$ by the coordination number ($z=4$) of the square lattice and accordingly, the spin-phonon coupling constants are four times larger than in Ref. 26. Assuming the Heisenberg model behaves also in the case of spin-$\frac{1}{2}$ like a weakly interacting Bose fluid[20,24,25] at low temperatures, we will develop in the following section a loop expansion or $1/S$ expansion in the perturbation theory around the spin-wave ground state, obtained via a Bogoliubov transformation.

C. Renormalized harmonic approximation

In the renormalized harmonic approximation only those diagrams are considered which make a contribution proportional to $1/S$, and accordingly, such an approximation is on the level of a self-consistent Hartree-Fock theory in fermion systems. The canonical Bogoliubov transformation, which diagonalizes the quadratic part of (9), is defined by

$$\begin{bmatrix}a_k\\b_{-k}^+\end{bmatrix}=\begin{bmatrix}u_k&-v_k\\-v_k&u_k\end{bmatrix}\begin{bmatrix}\alpha_k\\\beta_{-k}^+\end{bmatrix}\tag{12}$$

and their Hermitian conjugates, where u_k and v_k are Bogoliubov coefficients, which have to fulfill the following relation in order to be canonical:

$$u_k^2-v_k^2=1\ .\tag{13}$$

After the normal ordering of (9) with respect to the ground state obtained by the Bogoliubov transformation (12), we get a rather long Hamiltonian, which contains a constant term, a quadratic term, and a quartic term in Boson operators of the α and β type, weighted with nine vertex functions V^n ($n=1,\ldots,9$). These vertex functions and their symmetry properties are reported in Refs. 25 and 34, where we have to use the replacements $\gamma(\mathbf{k})\rightarrow\gamma'(\mathbf{k})$ and $N\rightarrow N/2$ (N in Refs. 25 and 34 refers to the total number of the Néel sublattice atoms). The Hamiltonian $\mathbf{H}^S$ can now be represented in the form

$$\begin{aligned}H_{\mathrm{DM}}^S=H_e\sum_k&\left\{\left[\gamma(\mathbf{k}_\parallel)A_\parallel(\tau=0)+\frac{\alpha_\perp}{2}\cos(k_z)A_\perp(\tau=0)\right][\eta(a_kb_{-k})+\eta(a_k^+b_{-k}^+)]\right.\\&\left.+\left[A_\parallel(\tau=0)+\frac{\alpha_\perp}{2}A_\perp(\tau=0)\right][\eta(a_k^+a_k)+\eta(b_{-k}^+b_{-k})]\right\}-\frac{H_e}{2NS}\sum_{k_1,k_2,k_3,k_4}\delta_G(\mathbf{k}_1+\mathbf{k}_2-\mathbf{k}_3-\mathbf{k}_4)\\&\times[V^1_{k_1k_2k_3k_4}\alpha_{k_1}^+\alpha_{k_2}^+\alpha_{k_3}\alpha_{k_4}+2V^2_{k_1k_2k_3k_4}\alpha_{k_1}^+\beta_{-k_2}\alpha_{k_3}\alpha_{k_4}+2V^3_{k_1k_2k_3k_4}\alpha_{k_1}^+\alpha_{k_2}^+\beta_{-k_4}\alpha_{k_3}\\&+4V^4_{k_1k_2k_3k_4}\alpha_{k_1}^+\beta_{-k_4}^+\alpha_{k_3}\beta_{-k_2}+2V^5_{k_1k_2k_3k_4}\beta_{-k_4}^+\beta_{-k_1}\alpha_{k_3}\beta_{-k_2}+2V^6_{k_1k_2k_3k_4}\alpha_{k_1}^+\beta_{-k_3}\beta_{-k_4}^+\beta_{-k_2}\\&+V^7_{k_1k_2k_3k_4}\alpha_{k_1}^+\alpha_{k_2}^+\beta_{-k_3}^+\beta_{-k_4}^++V^8_{k_1k_2k_3k_4}\beta_{-k_1}\beta_{-k_2}\alpha_{k_3}\alpha_{k_4}+V^9_{k_1k_2k_3k_4}\beta_{-k_3}^+\beta_{-k_4}^+\beta_{-k_1}\beta_{-k_2}]\ ,\end{aligned}\tag{14}$$

where $A_\parallel(\tau=0)$ and $A_\perp(\tau=0)$ are the in-plane and the out-of-plane renormalization constant of the spin-wave dispersion at zero temperature, respectively, and the reduced temperature is given by $\tau=k_BT/H_e$. Here η indicates normal ordering with respect to the ground state obtained by the Bogoliubov transformation (12). In (14)

the constant term has been dropped. At finite temperatures we have to take account of one-loop contributions of the quartic term in (14). That yields for H^S in RHA at finite temperatures, after diagonalization of the Hamiltonian (14), using the relations in (13) and (22) and inserting the Bogoliubov coefficients given in (19) below,

$$H^S_{\mathrm{DM}}(\mathrm{RHA}) = H_e A_{\parallel}(\tau)[1+r(\tau)] \times \sum_k \sqrt{1-\bar{\gamma}^2(\mathbf{k},\tau)}(\alpha_k^+\alpha_k + \beta_{-k}^+\beta_{-k}) . \tag{15}$$

Here the quasiparticle energies in RHA are given by

$$\epsilon(\mathbf{k},\tau) = H_e A_{\parallel}(\tau)[1+r(\tau)]\sqrt{1-\bar{\gamma}^2(\mathbf{k},\tau)} \tag{16}$$

and the following abbreviations have been introduced:

$$\bar{\gamma}(\mathbf{k},\tau) = \frac{\gamma(\mathbf{k}_{\parallel})}{1+r(\tau)} + \frac{r(\tau)}{1+r(\tau)}\cos(k_z) ,$$
$$r(\tau) = \frac{\alpha_{\perp} A_{\perp}(\tau)}{2A_{\parallel}(\tau)} . \tag{17}$$

The in-plane and the out-of-plane renormalization constants at finite temperatures obey the following self-consistent equations:

$$A_{\parallel}(\tau) = 1 + \frac{1}{NS}\sum_k \left[\frac{[\gamma(\mathbf{k}_{\parallel})\bar{\gamma}(\mathbf{k},\tau)-1][1+2n(\epsilon(\mathbf{k},\tau))]}{\sqrt{1-\bar{\gamma}^2(\mathbf{k},\tau)}} + 1 \right],$$
$$A_{\perp}(\tau) = 1 + \frac{1}{NS}\sum_k \left[\frac{[\cos(k_z)\bar{\gamma}(\mathbf{k},\tau)-1][1+2n(\epsilon(\mathbf{k},\tau))]}{\sqrt{1-\bar{\gamma}^2(\mathbf{k},\tau)}} + 1 \right], \tag{18}$$

where $n(\epsilon(\mathbf{k},\tau))$ denotes, as usual, the Bose distribution function. These results for the renormalization constants coincide with the formulas of Kopietz[22] in the ordered phase, who used Schwinger-boson mean-field theory to derive them. The Bogoliubov coefficients are defined by

$$u_k^2 + v_k^2 = \frac{1}{\sqrt{1-\bar{\gamma}^2(\mathbf{k},\tau)}}, \quad u_k v_k = \frac{1}{2}\frac{\bar{\gamma}(\mathbf{k},\tau)}{\sqrt{1-\bar{\gamma}^2(\mathbf{k},\tau)}}$$
$$u_k^2 = \frac{1}{2}\left[\frac{1}{\sqrt{1-\bar{\gamma}^2(\mathbf{k},\tau)}} + 1 \right], \tag{19}$$
$$v_k^2 = \frac{1}{2}\left[\frac{1}{\sqrt{1-\bar{\gamma}^2(\mathbf{k},\tau)}} - 1 \right] .$$

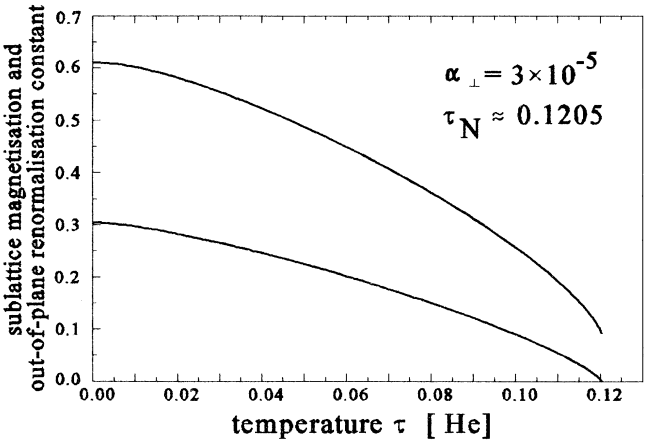

FIG. 1. Sublattice magnetization (lower curve) and out-of-plane renormalization constant (upper curve) in the framework of a renormalized harmonic approximation (self-consistent one-loop approximation), considering a weak exchange coupling between the layers. Using the parameters for La_2CuO_4 from Ref. 15 with $\alpha_{\perp}=3\times10^{-5}$, we obtain a Néel temperature of approximately 0.1205 ($\approx$ room temperature with $J\approx110$–130 meV) in reduced units. The out-of-plane renormalization constant vanishes slightly above τ_N. For a detailed discussion of the sublattice magnetization and the out-of-plane renormalization constant, see Ref. 22. The xy anisotropies, neglected in the model considered here, change the behavior close to the phase transition (Ref. 15) to xy behavior and higher loop corrections shift the Néel temperature to lower temperatures.

The in-plane renormalization constant is in the low-temperature limit approximately given by its 2D zero-temperature value of $1+0.158/2S$.[22,26] Note, however, that it is also fulfilled at room temperature in high-T_c superconductor basic materials because of the large in-plane exchange integral. The equation for the out-of-plane renormalization constant (18) was solved numerically and the results for the out-of-plane renormalization constant and the sublattice magnetization are shown in Fig. 1 in the ordered phase, choosing the experimental value $\alpha_{\perp}=3\times10^{-5}$ in the case of La_2CuO_4.[15] As can be seen, the dispersion of the spin waves is quasi-2D, because $r(\tau)$ decreases from approximately 8×10^{-6} at zero temperature to 1×10^{-6} at the Néel temperature. Accordingly, we can set later in the calculations of the one-magnon spectra function and the Raman cross section $r(\tau)$ equal to zero, because we are only interested in short-wavelength in-plane excitations. This yields a purely 2D spin system, where, however, the coupling of the 3D phonons onto the 2D spin systems is still present, i.e., the projection of the displacement operators onto the xy plane still modulates the in-plane exchange integral. Bilinearization of the spin-phonon part of the Hamiltonian, using the relations in (22) and the Bogoliubov transformation (12), yields

$$H_{\mathrm{DM}}^{\mathrm{SP}}(\mathrm{RHA})=-iBH_e A_{\parallel}(\tau)[1+r(\tau)]\sum_{k_1,k_2,q,j}\delta_G(\mathbf{k}_1-\mathbf{k}_2-\mathbf{q})\left[\frac{\hbar}{2Nm\omega_j(\mathbf{q})}\right]^{1/2}$$
$$\times\{[\bar{\Delta}(\mathbf{q},j,\mathbf{k}_2)-\bar{\Delta}(\mathbf{q},j,\mathbf{k}_2+\mathbf{q})]\eta(a_{k_1}b_{-k_2})$$
$$-[\bar{\Delta}(\mathbf{q},j,\mathbf{k}_1)-\bar{\Delta}(\mathbf{q},j,\mathbf{k}_1+\mathbf{q})]\eta(a_{k_2}^{+}b_{-k_1}^{+})$$
$$-\bar{\Delta}(\mathbf{q},j,\mathbf{q})\eta(a_{k_2}^{+}a_{k_1})-\bar{\Delta}(\mathbf{q},j,\mathbf{k}_1\mathbf{k}_2)\eta(b_{-k_1}^{+}b_{-k_2})\}u_j(\mathbf{q}) , \tag{20}$$

where we have defined

$$\bar{\Delta}(\mathbf{q},j,\mathbf{k})=\frac{1}{1+r(\tau)}\left[\frac{1}{2}\sum_{\alpha=x,y}e_\alpha(\mathbf{q},j)\sin(k_\alpha)+r(\tau)e_z(\mathbf{q},j)\sin(k_z)\right] . \tag{21}$$

As already pointed out above, we used in the derivation of (15) and (20) the following relations:

$$\sum_{k'}\gamma'(\mathbf{k}-\mathbf{k}')w(\mathbf{k}')=\gamma(\mathbf{k}_{\parallel})\sum_{k'}\gamma(\mathbf{k}'_{\parallel})w(\mathbf{k}')+\frac{\alpha_\perp}{2}\cos(k_z)\sum_{k'}\cos(k'_z)w(\mathbf{k}') ,$$
$$\sum_{k'}\Delta'(\mathbf{q},j,\mathbf{k}'+\mathbf{q})w(\mathbf{k}')=\Delta(\mathbf{q},j,\mathbf{q}_{\parallel})\sum_{k'}\gamma(\mathbf{k}'_{\parallel})w(\mathbf{k}')+\frac{\alpha_\perp}{2}e_z(\mathbf{q},j)\sin(q_z)\sum_{k'}\cos(k'_z)w(\mathbf{k}') , \tag{22}$$

where $w(\mathbf{k})$ is a function with tetragonal symmetry. Applying the Bogoliubov transformation (12) we obtain for the spin-phonon part of the Hamiltonian in RHA

$$H_{\mathrm{DM}}^{\mathrm{SP}}(\mathrm{RHA})=i\frac{H_e A_{\parallel}(\tau)[1+r(\tau)]}{\sqrt{N}}\sum_{k_1,k_2,q,j}\delta_G(\mathbf{k}_1-\mathbf{k}_2-\mathbf{q})\lambda_j$$
$$\times[g_{\alpha^+\alpha}(\mathbf{q},\mathbf{k}_1,\mathbf{k}_2,j)\alpha_{k_2}^{+}\alpha_{k_1}+g_{\beta^+\beta}(\mathbf{q},\mathbf{k}_1,\mathbf{k}_2,j)\beta_{-k_1}^{+}\beta_{-k_2}$$
$$+g_{\alpha^+\beta^+}(\mathbf{q},\mathbf{k}_1,\mathbf{k}_2,j)\alpha_{k_2}^{+}\beta_{-k_1}^{+}+g_{\alpha\beta}(\mathbf{q},\mathbf{k}_1,\mathbf{k}_2,j)\alpha_{k_1}\beta_{-k_2}]u_j(\mathbf{q}) , \tag{23}$$

where the vertex functions and their symmetry properties are given in the Appendix. The phonon spectrum is defined by

$$\hbar\omega_j(\mathbf{q})=\hbar\omega_j m(\mathbf{q}) \tag{24}$$

and $\hbar\omega_j$ represents a characteristic energy for the different acoustic-phonon modes and lies in the range of 20 meV; $m(\mathbf{q})$ represents the dispersion of the acoustic phonons. The dimensionless spin-phonon coupling constants are now defined by

$$\lambda_j=\frac{B}{H_e}(\hbar/2m\omega_j)^{1/2} . \tag{25}$$

As a consequence, we may initiate a perturbation theory, where the spin-phonon part in RHA and the contributions higher than $1/S$ of the spin part of the Hamiltonian ignored so far are considered perturbatively. The kinematic interaction, which comes from the restriction, that a lattice site cannot be occupied by more than $2S$ bosons, was ignored in the low-temperature regime,[20,21,25] and we considered only the dynamic interaction between the Bosons, resulting from the off-diagonal terms of the Boson Hamiltonian in the spin-wave eigenfunctions. In the Born approximation (BA) we get one-loop contributions, dressed by the mean-field approximation of the quartic part in the magnon operators, derived from the spin-phonon part[26] and two-loop contributions derived from the spin part.[20,21,25,34] In the next section we will derive the Dyson equation for the magnon propagator in BA.

III. BORN APPROXIMATION

In the temperature Green's-function formalism the magnon propagator and the phonon propagator are defined, respectively, by

$$G(\mathbf{k},z_\nu)=\begin{bmatrix}G_{11}(\mathbf{k},z_\nu) & G_{12}(\mathbf{k},z_\nu)\\ G_{21}(\mathbf{k},z_\nu) & G_{22}(\mathbf{k},z_\nu)\end{bmatrix}$$
$$=\frac{1}{i\hbar}\int_0^{-i\hbar\beta}dt\,e^{iz_\nu t}\left\langle T\begin{bmatrix}\alpha_k(t)\\ \beta_{-k}^{+}(t)\end{bmatrix}(\alpha_k^{+}(0)\beta_{-k}(0))\right\rangle , \tag{26}$$
$$D_j(\mathbf{q},z_\nu)=\frac{1}{i\hbar}\int_0^{-i\hbar\beta}dt\,e^{iz_\nu t}\langle Tu_j(\mathbf{q},t)u_j(-\mathbf{q},0)\rangle ,$$

where $z_\nu=i2\pi\nu/\beta\hbar$ represents a bosonic Matsubara frequency and ν is an integer. The irreducible self-energy of the magnons is defined by

$$\Sigma^*(\mathbf{k},z_\nu)=\begin{bmatrix}\Sigma_{11}^*(\mathbf{k},z_\nu) & \Sigma_{12}^*(\mathbf{k},z_\nu)\\ \Sigma_{21}^*(\mathbf{k},z_\nu) & \Sigma_{22}^*(\mathbf{k},z_\nu)\end{bmatrix} , \tag{27}$$

and due to the inversion symmetry of the lattice and the sublattice symmetry has the following symmetry proper-

ties:[34]

$$\Sigma^*_{11}(\mathbf{k},z_\nu)=\Sigma^*_{22}(-\mathbf{k},-z_\nu)\ ,$$
$$\Sigma^*_{12}(\mathbf{k},z_\nu)=\Sigma^*_{21}(-\mathbf{k},-z_\nu)\ . \tag{28}$$

The Dyson equation is of the form

$$G(\mathbf{k},z_\nu)=G^0(\mathbf{k},z_\nu)+G^0(\mathbf{k},z_\nu)\Sigma^*(\mathbf{k},z_\nu)G(\mathbf{k},z_\nu)\ . \tag{29}$$

$G^0(\mathbf{k},z_\nu)$ is the magnon propagator averaged with H^S_{DM} (RHA) yielding

$$G^0(\mathbf{k},z_\nu)=\begin{pmatrix}\dfrac{1}{\hbar z_\nu-\epsilon(\mathbf{k},\tau)} & 1\\ 1 & \dfrac{-1}{\hbar z_\nu+\epsilon(\mathbf{k},\tau)}\end{pmatrix}\ . \tag{30}$$

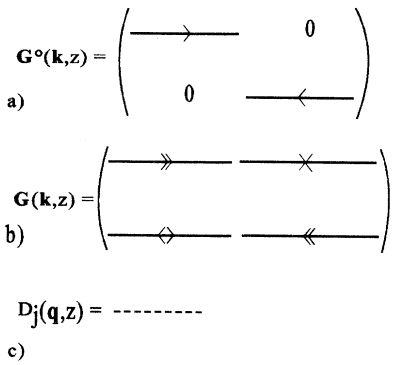

FIG. 2. Diagrammatic representation of the propagators, following their definition in (26). In (a) the unrenormalized magnon propagator, in (b) the full magnon propagator and in (c) the phonon propagator are shown.

Diagrammatically the propagators may be represented as shown in Fig. 2.

Considering now the spin-phonon part, we obtain for the self-energy in BA in the weak-coupling case, which applies for high-T_c superconductor basic materials,[26]

$$\Sigma^*(\mathbf{k},z_\nu)=-\frac{H_e A_\parallel(\tau)[1+r(\tau)]}{N\beta}\times\sum_{k_1,q,z_{\nu_1},j}\delta_G(\mathbf{k}_1-\mathbf{k}-\mathbf{q})\lambda_j^2 D_j(\mathbf{q},z_{\nu_1})$$
$$\times\{g^2_{\alpha^+\alpha}(\mathbf{q},\mathbf{k}_1,\mathbf{k},j)G^0(\mathbf{k}_1,z_\nu+z_{\nu_1})+g^2_{\alpha^+\beta^+}(\mathbf{q},\mathbf{k}_1,\mathbf{k},j)G^0(-\mathbf{k}_1,-z_\nu-z_{\nu_1})$$
$$+g_{\alpha^+\alpha}(\mathbf{q},\mathbf{k}_1,\mathbf{k},j)g_{\alpha\beta}(\mathbf{q},\mathbf{k}_1,\mathbf{k},j)[G^0(\mathbf{k}_1,z_\nu+z_{\nu_1})-G^0(-\mathbf{k}_1,-z_\nu-z_{\nu_1})]\tau_1\}\ , \tag{31}$$

where we have introduced the Pauli matrix τ_1 given by

$$\tau_1=\begin{bmatrix}0 & 1\\ 1 & 0\end{bmatrix}\ . \tag{32}$$

The unrenormalized phonon propagator in (31) is defined by

$$D_j(\mathbf{q},z_\nu)=\frac{2\hbar\omega_j(\mathbf{q})}{\hbar^2 z_\nu^2-\hbar^2\omega_j^2(\mathbf{q})}\ . \tag{33}$$

In the derivation of (31) we used some obvious symmetry properties recalled in the Appendix. Self-consistency can be achieved, if we make the substitution $G^0(\mathbf{k},z_\nu)\rightarrow G(\mathbf{k},z_\nu)$ and derive a self-consistent Dyson equation for the phonon propagator in BA, but due to the weak coupling of phonons onto magnons we may neglect self-consistency in the calculation of the one-magnon spectra function.

For similar reasons, we can approximate the Green's function for the α magnon by[34]

$$G_{11}(\mathbf{k},z_\nu)=\frac{1}{\hbar z_\nu-\epsilon(\mathbf{k},\tau)-\Sigma^*_{11}(\mathbf{k},z_\nu)} \tag{34}$$

and the Green's function for the β magnon is obtained via the symmetry properties listed in (28). The off-diagonal propagators may be ignored. After carrying out the frequency sum in (31) we can define a spectral representation of the self-energy Σ_{11} in the form

$$\tilde{\Sigma}^*_{11}(\mathbf{k},\tilde{z}_\nu)=\sum_{\sigma,j}\int_{-\infty}^{\infty}d\hbar\tilde{\omega}'\frac{S^{\sigma,j}_{\alpha^+\alpha}(\mathbf{k},\tilde{\omega}')+S^{\sigma,j}_{\alpha^+\beta^+}(\mathbf{k},\tilde{\omega}')}{\hbar z_\nu-\hbar\tilde{\omega}'}\ , \tag{35}$$

where σ runs over 0 and 1, and $\sigma=0$ and $\sigma=1$ indicate absorption and emission of a phonon, respectively (see Fig. 3), and the tilde indicates reduced units, i.e., we measure energies in units of H_e. The spectral functions in (35) are defined by

$$S^{\sigma j}_{\alpha^+\alpha}(\mathbf{k},\tilde{\omega})=\lim_{\delta\rightarrow 0^+}\frac{1}{\pi}\mathrm{Im}\tilde{\Sigma}^{*\sigma j}_{\alpha^+\alpha}(\mathbf{k},\tilde{\omega}-i\delta)\ ,$$
$$S^{\sigma j}_{\alpha^+\beta^+}(\mathbf{k},\tilde{\omega})=\lim_{\delta\rightarrow 0^+}\frac{1}{\pi}\mathrm{Im}\tilde{\Sigma}^{*\sigma j}_{\alpha^+\beta^+}(\mathbf{k},\tilde{\omega}-i\delta)\ , \tag{36}$$

yielding for the damping and the renormalization of the

dispersion of the magnons, respectively,

$$\tilde{\Gamma}_{11}(\mathbf{k},\tilde{\omega})=\mathrm{Im}\tilde{\Sigma}^{*}_{11}(\mathbf{k},\tilde{\omega})$$
$$=\sum_{\sigma j}\pi[S^{\sigma j}_{\alpha^{+}\alpha}(\mathbf{k},\tilde{\omega})+S^{\sigma j}_{\alpha^{+}\beta^{+}}(\mathbf{k},\tilde{\omega})]\ ,$$
$$\Delta\tilde{\epsilon}_{11}(\mathbf{k},\tilde{\omega})=\mathrm{Re}\tilde{\Sigma}^{*}_{11}(\mathbf{k},\tilde{\omega}) \tag{37}$$
$$=\sum_{\sigma j}P\int_{-\infty}^{\infty}d\hbar\tilde{\omega}'\frac{S^{\sigma j}_{\alpha^{+}\alpha}(\mathbf{k},\tilde{\omega}')+S^{\sigma j}_{\alpha^{+}\beta^{+}}(\mathbf{k},\tilde{\omega}')}{\hbar\tilde{\omega}-\hbar\tilde{\omega}'}\ ,$$

where P indicates the principal value. The diagrams for Σ_{11} are shown in Fig. 3. For the one-magnon spectral function $A_{11}(\mathbf{k},\omega)$ we obtain

$$A_{11}(\mathbf{k},\tilde{\omega})=\frac{1}{\pi}\mathrm{Im}G_{11}(\mathbf{k},\tilde{\omega})$$
$$=\tilde{A}_{11}(\mathbf{k},\tilde{\omega})/H_e$$
$$=\frac{1}{H_e\pi}\frac{\tilde{\Gamma}_{11}(\mathbf{k},\tilde{\omega})}{[\hbar\tilde{\omega}-\tilde{\epsilon}(\mathbf{k},\tau)-\Delta\tilde{\epsilon}_{11}(\mathbf{k},\tilde{\omega})]^2+\tilde{\Gamma}^2_{11}(\mathbf{k},\tilde{\omega})}$$
$$=-A_{22}(\mathbf{k},-\tilde{\omega})\ . \tag{38}$$

As shown in Refs. 26 and 31 only the first diagram in Fig. 3 yields a damping of on-shell magnons, i.e., $\hbar\omega=\epsilon(\mathbf{k},\tau)$, in the regime, where the sound velocities are smaller than the magnon velocities. This applies to high-T_c superconductor basic materials and because we are interested in the damping of high-energy magnons, we can neglect the $\sigma=0$ term in the first term of (35), which does not produce a damping of high-energy on-shell magnons. This allows us to concentrate on the spontaneous decay process, represented by the first term of (35) with $\sigma=1$, yielding for the spectral function of the self-energy

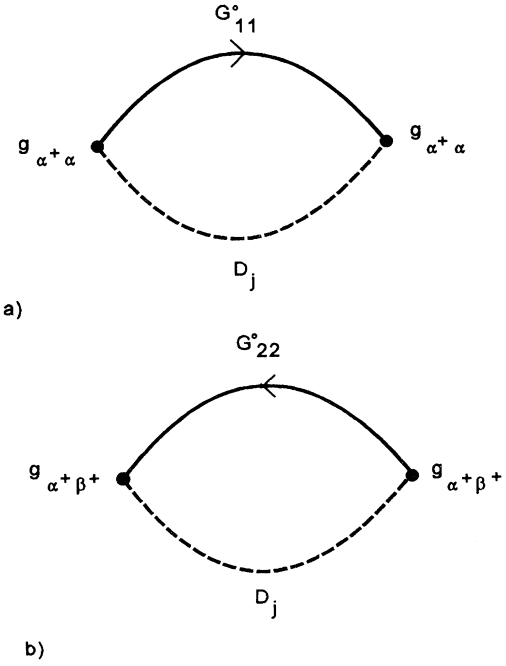

FIG. 3. Self-energy Σ_{11} in BA due to spin-phonon interaction, where in the case of sound velocities small compared to the magnon velocities only the diagram in (a) provides a damping of on-shell magnons. Each diagram can now be divided in two parts, where in (a) a given α magnon absorbs or emits a phonon and is scattered into another on-shell α magnon. In (b) a given α magnon absorbs an on-shell β magnon and absorbs and emits a phonon. The third diagram yields no damping of on-shell magnons, because the energy conservation can only be fulfilled by off-shell magnons with negative magnon energies. As a result that diagram can always be neglected. The fourth diagram yields a damping only, if the sound velocities are larger than the magnon velocities, which is not the case in the systems considered here.

$$S^{\sigma=1j}_{\alpha^{+}\alpha}(\mathbf{k},\tilde{\omega})=A^{2}_{\parallel}(\tau)[1+r(\tau)]^2\sum_{k_1 q}\delta_G(\mathbf{k}_1-\mathbf{k}-\mathbf{q})\lambda^2_j g^2_{\alpha^{+}\alpha}(\mathbf{q},\mathbf{k}_1,\mathbf{k},j)(1-e^{-\hbar\tilde{\omega}/\tau})[n(\hbar\tilde{\omega}_j(\mathbf{q}))+1][n(\tilde{\epsilon}(\mathbf{k}_1,\tau))+1]$$
$$\times\delta[\hbar\tilde{\omega}-\tilde{\epsilon}(\mathbf{k}_1,\tau)-\hbar\tilde{\omega}_j(\mathbf{q})]\ . \tag{39}$$

Neglecting the exchange coupling between the layers, the spectral functions in (38) and (39) will be independent of k_z. Observing the Hohenberg-Mermin-Wagner theorem,[35,36] implying there is no long-range order at finite temperatures for a 2D Heisenberg antiferromagnet, the calculations have to be restricted to wave numbers $\mathbf{k}\gg\xi^{-1}$, where ξ is the 2D correlation length and their temperature dependence is given by Ref. 19. For high-energy magnons this restriction is always fulfilled up to very high temperatures.

In a recent publication[26] we showed that the renormalization of spin waves in the long-wavelength and low-temperature limit in a 2D system is small and only in the short-wavelength limit we obtain a significant damping due to spin-phonon interaction for the case that sound velocities are small compared to the magnon velocities. Here we consider only the short-wavelength limit and some results for the one-magnon spectral function at the BZB, in particular, the damping and the renormalization of the spin-wave dispersion at zero temperature in the case of spin-$\frac{1}{2}$, are shown in Fig. 4. Account is taken only of longitudinally polarized phonons, i.e., $\mathbf{e}(\mathbf{q},j)\|\mathbf{q}$, which provide the leading contribution[26] to the renormalization of the spin waves, using $\lambda_L=0.1$ and the analogous 3D phonon dispersion to that employed in Ref. 26.

As can be seen in Fig. 4(a), the damping increases with increasing off-shell magnon energy, because the long-wavelength phonons become more important, until a maximum energy, which is higher than the on-shell magnon energy. Beyond this maximum, energy scattering via

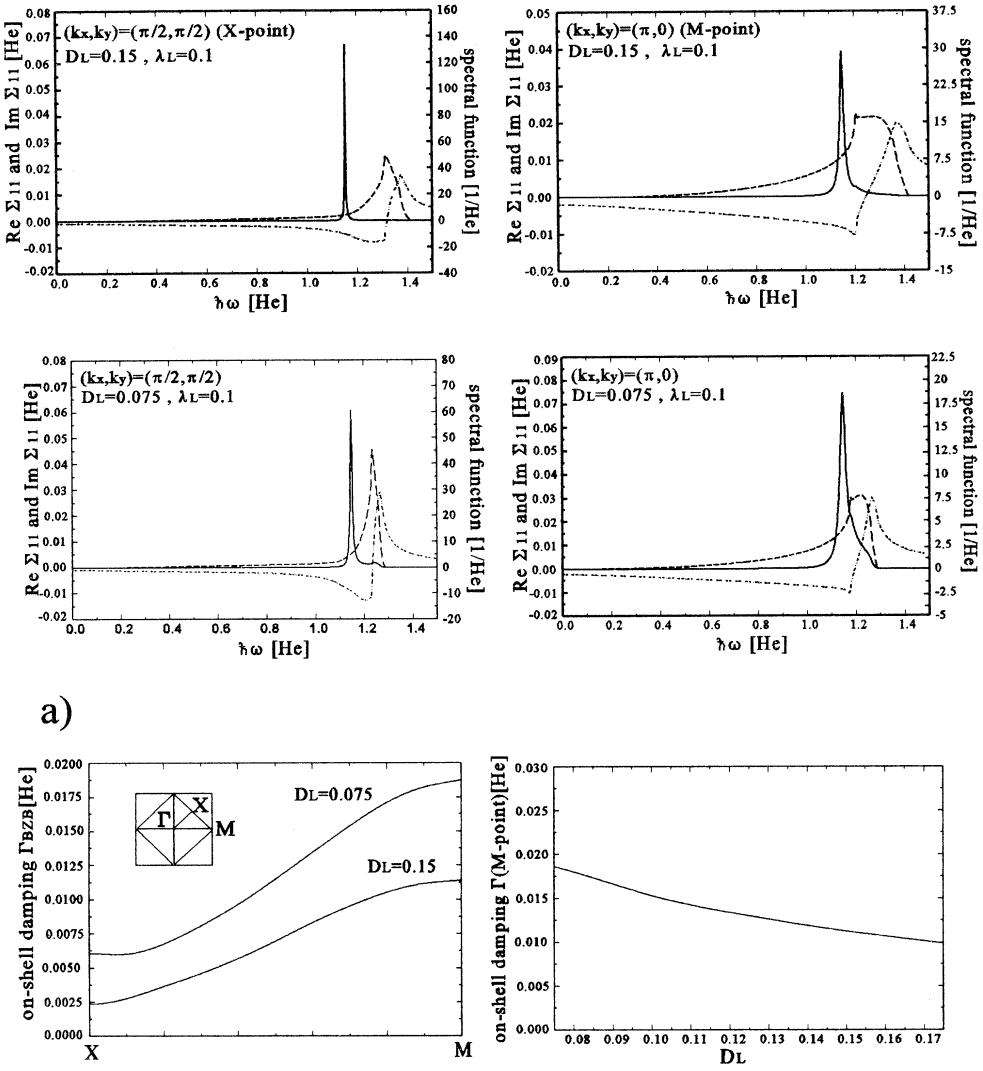

FIG. 4. (a) Imaginary (dashed line) and real (dashed-dotted line) part of the self-energy $\Sigma_{11}(\mathbf{k},\omega)$ (left scale) and spectral function (solid line and right scale) at zero temperature in the case of spin-$\frac{1}{2}$ for different wave vectors $\mathbf{k}$ on the BZB, where only longitudinally acoustic phonons are considered. In the case of La_2CuO_4 we choose for the parameter $D_L=\hbar\omega_L/H_e$ the value 0.075 with $\hbar\omega_L=17$ meV and $H_e=230$ meV. We used the in-plane exchange integral $H_e^{\text{eff}}\approx 266$ meV from the Raman-scattering experiments from Ref. 7, yielding $H_e=H_e^{\text{eff}}/A_{\parallel}(\tau=0)\approx 230$ meV. The parameter $D_L=0.15$ coincides with $H_e\approx 115$ meV. For the spin-phonon coupling constants we choose the value 0.1 (that coincides with $\lambda_L=0.025$ in our old notation, used in Ref. 26). (b) On-shell damping (left figure) on the BZB for $D_L=0.075$ and $D_L=0.15$, showing the anisotropy of the damping and on-shell damping at the M point (right figure) as a function of D_L, showing the decrease of the damping with increasing D_L or decreasing H_e, respectively.

long-wavelength phonons will be even more impossible with increasing energy and the damping decreases until the damping will be zero, because energy and momentum conversation cannot be fulfilled. The real part of the self-energy changes its sign from a negative shift to a positive shift of the spin-wave dispersion close to the maximum damping energy. As a consequence, the peak position of the spectral function is shifted to lower energies, but this shift is very small (lower than one percent of the on-shell magnon energy) and may be neglected. In Fig. 4(b) we show in the left-hand part of the figure the anisotropy of the damping from the X point to the M point. The damping increases from the X point to the M point, because at the M point more long-wavelength acoustic phonons are involved in the scattering process. In the right-hand side of the figure the decrease of the damping at the M point is shown with increasing D_L, which represents the ratio of the characteristic energy of longitudinally acoustic phonons to the characteristic energy of the magnetic system H_e. Assuming the characteristic phonon energy to be a slowly varying function between the different compounds, the ratio between the two energies is fixed by the characteristic energy of the magnetic system H_e. Consequently, the damping increases with increasing exchange integral. The spin-phonon coupling constants were also assumed to be slowly varying functions of the lattice parameters, because the ratio of the gradient of the exchange integral to the exchange integral is proportional to $1/a$ (a represents the in-plane lattice constant), assuming a power law for the effective exchange integral $J\sim 1/r^n$ (n real number),[8] yielding slowly varying spin-phonon coupling constants as a function of the lattice parameters. In comparison to our former, plainly 2D result,[26] the on-shell damping is approximately a factor of 2 smaller, mainly to the increase of the phonon energies with increasing out-of-plane momentum q_z, resulting in a decrease of the vertex function $[\approx 1/m(\mathbf{q})^{1/2}]$. Evaluating the $1/S^2$ contributions, coming from the intrinsic spin part of the Hamiltonian, Harris *et al.*[34] obtained for the spectral function of the self-energy Σ_{11}, considering only that part of the self-energy which yields a damping of on-shell magnons,

$$S_{11}^{22}(\mathbf{k},\tilde{\omega})=\left[\frac{1}{2NS}\right]^2\sum_{k_2,k_3,k_4}\delta_G(\mathbf{k}+\mathbf{k}_2-\mathbf{k}_3-\mathbf{k}_4)[8V^1_{kk_2k_3k_4}V^1_{k_3k_4kk_2}+16V^4_{k-k_4k_3-k_2}V^4_{k_3-k_2k-k_4}]$$
$$\times(1-e^{-\hbar\tilde{\omega}/\tau})n(\tilde{\epsilon}(\mathbf{k}_2,\tau))[n(\tilde{\epsilon}(\mathbf{k}_3,\tau))+1][n(\tilde{\epsilon}(\mathbf{k}_4,\tau))+1] \quad (40)$$
$$\times\delta[\hbar\tilde{\omega}+\tilde{\epsilon}(\mathbf{k}_2,\tau)-\tilde{\epsilon}(\mathbf{k}_3,\tau)-\tilde{\epsilon}(\mathbf{k}_4,\tau)]\ .$$

Because energy and momentum conservation cannot be fulfilled by spontaneous decay processes for on-shell magnons, damping of on-shell magnons at zero temperature due to the intrinsic spin part of the Hamiltonian does not exist. This is in contrast to spin-phonon interaction[26,31] in the regime that sound velocities are smaller than magnon velocities. Tyč and Halperin[20] calculated the damping of magnons in a 2D Heisenberg antiferromagnet in the long-wavelength and low-temperature limit, using formula (40), and made a self-consistent check for off-shell magnons. As a result, they obtain that magnons are well defined quasiparticles also in the case $S=\frac{1}{2}$ in the regime $k\gg\xi^{-1}$, because the damping is small compared to the magnon energies. Kopietz calculated the damping of high-energy magnons, using the same formula (40), and obtained for the damping[21]

$$\tilde{\Gamma}_{11}(\mathbf{k},\tilde{\epsilon}(\mathbf{k},\tau)/\hbar)=\frac{4\pi Z(|v_k|)\tau^3}{3S^2}\ , \quad (41)$$

where v_k is the gradient of the magnon dispersion and the function Z is approximately unity close to the BZB. As a consequence, the damping of magnons due to the intrinsic spin part can be neglected at low temperatures and the main contribution comes from spin-phonon interaction in the regime where sound velocities are smaller than magnon velocities. If the sound velocities are not much smaller than magnon velocities, spin-phonon interaction may also be neglected and the spectral functions are very narrow, yielding perfect quasiparticles. In the next section we calculate the two-magnon Raman cross section due to nearest-neighbor spin-pair excitations, using the formalism presented in this section, and compare our results with the measured B_{1g} mode.

IV. TWO-MAGNON RAMAN CROSS SECTION

First, we repeat shortly the derivation of the two-magnon Raman cross section for the B_{1g} mode in the framework of a ladder approximation (RHA), following Davies, Chinn, and Zeiger[4] and Canali and Girvin.[25] Neglecting the exchange coupling between layers, the effective Raman-scattering Hamiltonian for the B_{1g} mode, considering a square lattice, where only isotropic nearest-neighbor spin-pair excitations are involved in the scattering process, is given by[2-4]

$$H_{B_{1g}}=C\sum_{l,\delta}[\tfrac{1}{2}\mathbf{E}_i\cdot\mathbf{E}_f-(\mathbf{E}_i\cdot\delta)(\mathbf{E}_f\cdot\delta)]\mathbf{S}_l\cdot\mathbf{S}_{l+\delta}\ . \quad (42)$$

Here $\mathbf{E}_i$ and $\mathbf{E}_f$ are the incident and the scattered electric-field vectors, respectively. The δ summation in (42) runs over the nearest neighbors on a square lattice. The prefactor C, in the case of the one-band Hubbard model,[2] is proportional to $t^2/(U-\hbar\omega_i)$, where ω_i is the frequency of the incident light and t and U are the hopping and the repulsion term of the one-band Hubbard model, respectively. If the incident energy of the laser light is very different from the repulsion term, we would get only spin-pair excitations on neighboring sites, represented by the Hamiltonian in (42), and we could neglect higher-order corrections, yielding finite Raman cross sections in A_{1g} and B_{2g} symmetry and higher contributions in the effective Raman-scattering Hamiltonian of the B_{1g} mode. Here we are only concerned with the problem of the Raman spectrum of the B_{1g} mode generated by spin-pair excitations on neighboring sites, which dominate the low-energy side of the whole Raman spectrum. Higher-order processes are neglected. They are produced by the resonant enhancement of the Raman cross section in the real systems via the resonant excitation of transitions close to the charge-transfer gap $E_{\mathrm{CTG}}\approx 1.7$ eV,[28] i.e., we need to consider higher contributions in the $t/(U-\hbar\omega_i)$ expansion. That resonant enhancement can also be seen in the formulas of Shastry and Shraiman,[2] if the repulsion term of the one-band Hubbard model U is replaced by the effective charge-transfer gap E_{CTG} in the framework of an effective one-band Hubbard model.[2,27]

After the bosonization of the scattering Hamiltonian (42), using the Dyson-Maleev transformation (5,6) and the Bogoliubov transformation (12), we obtain an effective two-magnon scattering Hamiltonian in RHA,[4,25] where we have dropped the four-magnon contributions and due to the dominance of short-wavelength excitations we neglected terms proportional to u_kv_k, which are small close to the BZB,[4]

$$H_{B_{1g}}(\text{two-magnon})=CSA_{\parallel}(\tau)M(\mathbf{E}_i,\mathbf{E}_f)\sum_k f(\mathbf{k})(u_k^2+v_k^2)(\alpha_k^+\beta_{-k}^+ +\alpha_k\beta_{-k})$$
$$\equiv CSA_{\parallel}(\tau)M(\mathbf{E}_i,\mathbf{E}_f)\sum_k \bar{f}(\mathbf{k})(\alpha_k^+\beta_{-k}^+ +\alpha_k\beta_{-k})\ . \quad (43)$$

The sum in (43) runs over the 2D magnetic Brillouin zone, which is defined with respect to the square lattice. The symmetry functions of the B_{1g} mode $M(\mathbf{E}_i,\mathbf{E}_f)$ and $f(\mathbf{k})$ are given, respectively, by

$$M(\mathbf{E}_i,\mathbf{E}_f)=E_i^y E_f^y-E_i^x E_f^x\ ,$$
$$f(\mathbf{k})=\cos(k_x)-\cos(k_y)\ . \tag{44}$$

The generalized susceptibility $\chi(t)$, considering only terms which contribute in the noninteracting case,[4,25] may be defined by

$$\chi(t)=\frac{2}{N}\sum_{k,k'}\bar{f}(\mathbf{k})\bar{f}(\mathbf{k}')\times\left[\frac{1}{i\hbar}\langle T\alpha_k^+(t)\beta_{-k}^+(t)\alpha_{k'}(0)\beta_{-k'}(0)\rangle+\frac{1}{i\hbar}\langle T\alpha_k(t)\beta_{-k}(t)\alpha_{k'}^+(0)\beta_{-k'}^+(0)\rangle\right]$$
$$\equiv\frac{2}{N}\sum_{k,k'}\bar{f}(\mathbf{k})\bar{f}(\mathbf{k}')[\chi_{kk'}^-(t)+\chi_{kk'}^+(t)]\ . \tag{45}$$

After Fourier transformation, we obtain for the susceptibility

$$\chi(z_\nu)=\frac{2}{N}\sum_{k,k'}\bar{f}(\mathbf{k})\bar{f}(\mathbf{k}')[\chi_{kk'}^+(-z_\nu)+\chi_{kk'}^+(z_\nu)]$$
$$\equiv\chi^+(-z_\nu)+\chi^+(z_\nu)\ , \tag{46}$$

where we used the symmetry property[25]

$$\chi_{kk'}^-(z_\nu)=\chi_{kk'}^+(-z_\nu)\ . \tag{47}$$

Applying the fluctuation-dissipation theorem[37] we obtain for the dynamic structure factor, which is proportional to the Raman cross section

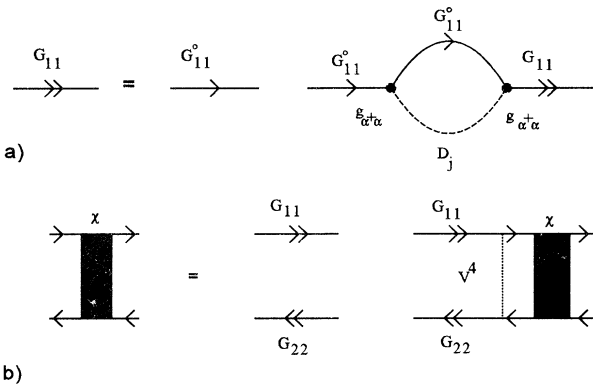

FIG. 5. Diagrammatic representation of the approximations, used to calculate the two-magnon Raman cross section. (a) The magnon propagator for the α magnon, where only the first diagram shown in Fig. 3, has been considered. Close to BZB only the spontaneous decay process has to be considered. Using the symmetry properties, one can show analogously the diagrammatic representation for the β magnon. (b) Bethe-Salpeter equation for the two-magnon propagator in RHA, where the one-magnon propagators are given via the Dyson equation, shown in (a). Due to the weak coupling of the phonons onto the magnons, vertex corrections due to spin-phonon interaction in the Bethe-Salpeter equation are neglected.

$$S(\omega)=\frac{1}{\pi}\frac{\mathrm{Im}\chi^+(-\omega+i\delta^+)+\mathrm{Im}\chi^+(\omega-i\delta^+)}{1-e^{-\beta\hbar\omega}}$$
$$\approx\frac{1}{\pi}\mathrm{Im}\chi^+(\omega-i\delta^+)\ , \tag{48}$$

where the last relation holds in the case $\hbar\omega\gg k_BT$ (only Stokes processes are possible). That is the case in the relevant energy regime considered here, because the magnons, which dominate the two-magnon spectral feature, are high-energy magnons, close to the BZB with a large two-magnon density of states.

Considering the spin part of the Hamiltonian, we get in RHA the following Bethe-Salpeter equation:

$$\chi^+(z_\nu)=P^{2+}(z_\nu)-\frac{H_e}{S}\left[\frac{2}{N}\right]^2\sum_{kk_1k_2k'}\bar{f}(\mathbf{k})P_{kk_1}^+(z_\nu)V_{k_1k_2k_2k_1}^4\bar{f}(\mathbf{k}')\chi_{k_2k'}^+(z_\nu)\ . \tag{49}$$

Here the abbreviations have been used

$$P^{2+}(z_\nu)=-\frac{1}{\beta}\frac{2}{N}\sum_{k,k',z_{\nu_1}}\bar{f}(\mathbf{k})\bar{f}(\mathbf{k}')G_{11}(\mathbf{k},z_{\nu_1})G_{22}(\mathbf{k},z_{\nu_1}-z_\nu)\delta_{k,k'}\equiv\frac{2}{N}\sum_{k,k'}\bar{f}(\mathbf{k})\bar{f}(\mathbf{k}')P_{k,k'}^+(z_\nu) \tag{50}$$

and the vertex function $V_{k1k2k2k1}^4$ is given by

$$V_{k_1k_2k_2k_1}^4=\frac{1}{2}\gamma(\mathbf{k}_1-\mathbf{k}_2)\left[\frac{1}{\sqrt{1-\gamma^2(\mathbf{k}_1)}\sqrt{1-\gamma^2(\mathbf{k}_2)}}+1\right]-\frac{1}{2}\frac{\gamma(\mathbf{k}_1)\gamma(\mathbf{k}_2)}{\sqrt{1-\gamma^2(\mathbf{k}_1)}\sqrt{1-\gamma^2(\mathbf{k}_2)}}\ . \tag{51}$$

Due to the weak coupling of phonons onto magnons, we neglect the scattering of two magnons by phonons and consider only the renormalization of the one-magnon spectral function due to spin-phonon interaction. As a result, we neglect vertex corrections due to spin-phonon interaction in the Bethe-Salpeter equation, yielding the same Bethe-Salpeter equation as in the case without spin-phonon interaction, but with renormalized one-magnon Green's functions. Diagrammatically, such an approximation is shown in Fig. 5. After straightforward calculations[4,25] we obtain

$$\chi^{+}(z_\nu)=\frac{P^{2+}(z_\nu)+H_e/8S[P^{0+}(z_\nu)P^{2+}(z_\nu)-(P^{1+}(z_\nu))^2]}{1+H_e/8S[P^{0+}(z_\nu)+P^{2+}(z_\nu)]+(H_e/8S)^2[P^{2+}(z_\nu)P^{0+}(z_\nu)-(P^{1+}(z_\nu))^2]} \ . \tag{52}$$

with the abbreviations

$$P^{1+}(z_\nu)=\frac{2}{N}\sum_{k,k'}\bar{f}(\mathbf{k})f(\mathbf{k})P^{+}_{k,k'}(z_\nu) \ ,$$
$$P^{0+}(z_\nu)=\frac{2}{N}\sum_{k,k'}f(\mathbf{k})f(\mathbf{k})P^{+}_{k,k'}(z_\nu) \ . \tag{53}$$

As shown by Canali and Girvin,[25] the Raman line remains nearly unchanged, if we set $u_k^2+v_k^2\approx 1$ close to the BZB, yielding

$$\chi(z_\nu)=\frac{P^{0+}(z_\nu)}{1+(H_e/4S)P^{0+}(z_\nu)} \tag{54}$$

or in reduced units

$$\tilde{\chi}^{+}(\tilde{z}_\nu)=\frac{p^{0+}(\tilde{z}_\nu)}{1+(1/4S)p^{0+}(\tilde{z}_\nu)}=\chi(\tilde{z}_\nu)/H_e \ . \tag{55}$$

Evaluating the frequency sums in (50) and (53), using the one-magnon spectral function, defined in (38), we may define the following spectra representations ($n=0,1,2$) in reduced units:

$$p^{n+}(\tilde{z}_\nu)=\int_{-\infty}^{\infty}d\hbar\tilde{\omega}'\frac{\bar{p}^{n}(\tilde{\omega}')}{\hbar\tilde{z}'_\nu-\hbar\tilde{\omega}'} \ , \tag{56}$$

where the spectral functions enter

$$\bar{p}^{0}(\tilde{\omega}')=\frac{2}{N}\sum_{k}f(\mathbf{k})f(\mathbf{k})\int_{-\infty}^{\infty}d\hbar\tilde{\omega}'_1[1+n(\hbar\tilde{\omega}'-\hbar\tilde{\omega}'_1)+n(\hbar\tilde{\omega}'_1)]\tilde{A}_{11}(\mathbf{k},\tilde{\omega}'-\tilde{\omega}'_1)\tilde{A}_{11}(\mathbf{k},\tilde{\omega}'_1) \ ,$$
$$\bar{p}^{1}(\tilde{\omega}')=\frac{2}{N}\sum_{k}\bar{f}(\mathbf{k})f(\mathbf{k})\int_{-\infty}^{\infty}d\hbar\tilde{\omega}'_1[1+n(\hbar\tilde{\omega}'-\hbar\tilde{\omega}'_1)+n(\hbar\tilde{\omega}'_1]\tilde{A}_{11}(\mathbf{k},\tilde{\omega}'-\tilde{\omega}'_1)\tilde{A}_{11}(\mathbf{k},\tilde{\omega}'_1) \ , \tag{57}$$
$$\bar{p}^{2}(\tilde{\omega}')=\frac{2}{N}\sum_{k}\bar{f}(\mathbf{k})\bar{f}(\mathbf{k})\int_{-\infty}^{\infty}d\hbar\tilde{\omega}'_1[1+n(\hbar\tilde{\omega}'-\hbar\tilde{\omega}'_1)+n(\hbar\tilde{\omega}'_1)]\tilde{A}_{11}(\mathbf{k},\tilde{\omega}'-\tilde{\omega}'_1)\tilde{A}_{11}(\mathbf{k},\tilde{\omega}'_1) \ .$$

Here we may drop the Bose distribution functions due to the dominance of high-energy magnons. As a result, the temperature dependence of the Raman cross section is governed by the temperature dependence of the one-magnon spectral function. Due to the weak renormalization of the dispersion of the spin waves, we may ignore the real part of the self-energy and consider only the damping of the spin waves with an effective in-plane exchange integral. Accordingly, the temperature dependence of the Raman cross section is only determined by the temperature dependence of damping. In order to handle the theory with a single nonuniversal parameter only and due to the dominance of BZB magnons, we define an over the BZB averaged on-shell damping parameter $\langle\Gamma(\mathbf{k},\epsilon(\mathbf{k},\tau)/\hbar)\rangle_{\mathrm{BZB}}$ within that approximation. The results for the two-magnon Raman cross section are shown in Fig. 6 for spin-$\frac{1}{2}$, spin-1, and spin-∞ (the noninteracting case), respectively, using different damping parameters. The peak positions shifts only slightly to lower energies with increasing damping and accordingly, the peak positions, measured in the experiments, provide a reliable estimate of the in-plane exchange integral. On the other hand, the peak intensity decreases quickly with increasing damping and the spectrum will be broadened. Consequently, if there are nearly undamped magnons at zero temperatures, we obtain a narrow line at zero temperature and we would get a rapid decrease of the peak intensity due to temperature-dependent damping effects due to spin-spin interaction, i.e., with a damping of 0.05 in reduced units at room temperature, there is a decrease of approximately 50% of the zero-temperature peak intensity. On the other hand, if there is a significant damping at zero temperature due to spin-phonon interaction, the Raman spectrum is broadened at zero temperature and the decrease with temperature is not so fast, i.e., with a damping of 0.05 in reduced units at zero temperature and a damping of 0.1 in reduced units at room temperature, there is only a decrease of approximately 20% of the zero-temperature peak intensity. The peak positions are given approximately by 1.69, 1.845, and 2 in reduced units in the case of spin-$\frac{1}{2}$, spin-1, and in the noninteracting case. The "excitonic" binding energy, defined by $2\times A_{\parallel}(\tau=0)-\hbar\tilde{\omega}_{\text{two-magnon peak}}$ behaves in the opposite way, it decreases from 0.626 (spin-$\frac{1}{2}$) over 0.313 (spin-1) to zero (noninteracting case).

In order to interpret the experiments, we calculate the averaged damping parameter as a function of the temperature for different parameters $D_L=\hbar\omega_L/H_e$, considering only longitudinally polarized phonons. The results in the case of spin-$\frac{1}{2}$ and spin-1 are shown in Fig. 7. The damping decreases with increasing D_L or decreasing H_e, showing that spin-phonon interaction is only effective in the regime where sound velocities are small compared to the magnon velocities. We assume, that the spin-phonon coupling constants and the characteristic phonon energies are slowly varying functions of the lattice parameters and accordingly we choose the same phonon parameters for the different substances. Based on that property we may estimate the damping of BZB magnons for different substances. In the case of La_2CuO_4 (spin-$\frac{1}{2}$) with $H_e=230$ meV and $D_L=0.075$, and Pr_2NiO_4 (spin-1) with

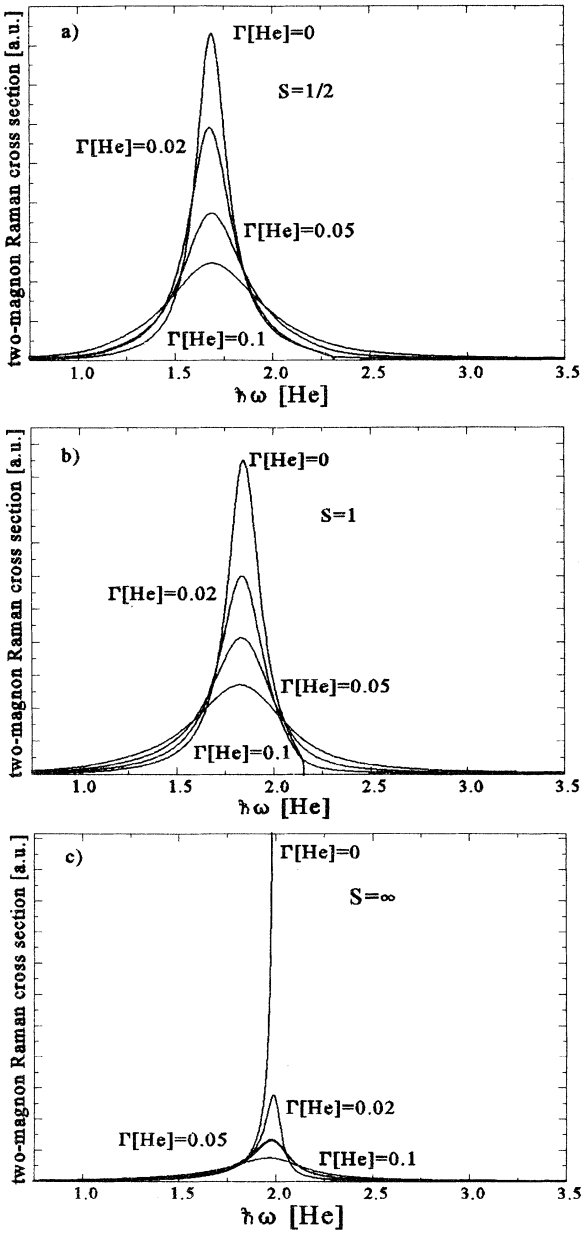

FIG. 6. Two-magnon Raman cross section, using different damping parameters, in the case of (a) spin-$\frac{1}{2}$ and (b) spin-1 and (c) in the noninteracting case ($S \rightarrow \infty$) (see text for discussion).

$H_e = 185$ meV and $D_L = 0.085$, respectively, we obtain at room temperature $\tau \approx 0.11$ an averaged damping of approximately 12 meV ($\Gamma/H_e \approx 0.052$) in the case of La_2CuO_4 (see the experiment of Singh *et al.*[7]) and at a temperature of 75 K ($\tau = 0.035$, see the experiment of de Andrés, Martinez, and Odier[13]) in the case of Pr_2NiO_4 a damping of 3.3 meV ($\Gamma/H_e \approx 0.018$). Here we have added the damping due to spin-phonon interaction (7 and 3.3 meV, respectively) with $\lambda_L = 0.1$ and spin-spin interaction (5 and 0.03 meV, respectively), using the formula derived by Kopietz (41). In the case of La_2NiO_4 (spin-1) with $H_e = 111$ meV and $D_L = 0.15$, we obtain for the damping at 30 K ($\tau = 0.023$, see the experiment of Sugai *et al.*[9]) 0.67 meV ($\Gamma/H_e \approx 0.006$) and at 75 K ($\tau = 0.058$) 0.8 meV ($\Gamma/H_e \approx 0.007$), which is much smaller than in the case of Pr_2NiO_4. Note that we get a damping of approximately 8 meV ($\Gamma/H_e \approx 0.072$) at room temperature ($\tau = 0.23$) in La_2NiO_4, which is mainly due to the temperature-dependent damping due to spin-spin interaction, and in Pr_2NiO_4 a damping at room temperature of 9 meV ($\Gamma/H_e \approx 0.05$), which is mainly due to spin-phonon interaction. This result explains the rapid decrease of the peak intensity of the two-magnon line in La_2NiO_4 as reported by Sugai *et al.*[9] Consequently, we get for all spin-$\frac{1}{2}$ substances and the spin-1 substance Pr_2NiO_4 nearly the same damping of BZB magnons. In the case of La_2NiO_4 the damping at low temperature is much smaller, yielding there a much smaller two-magnon Raman line at low temperatures as in the case of the cu-

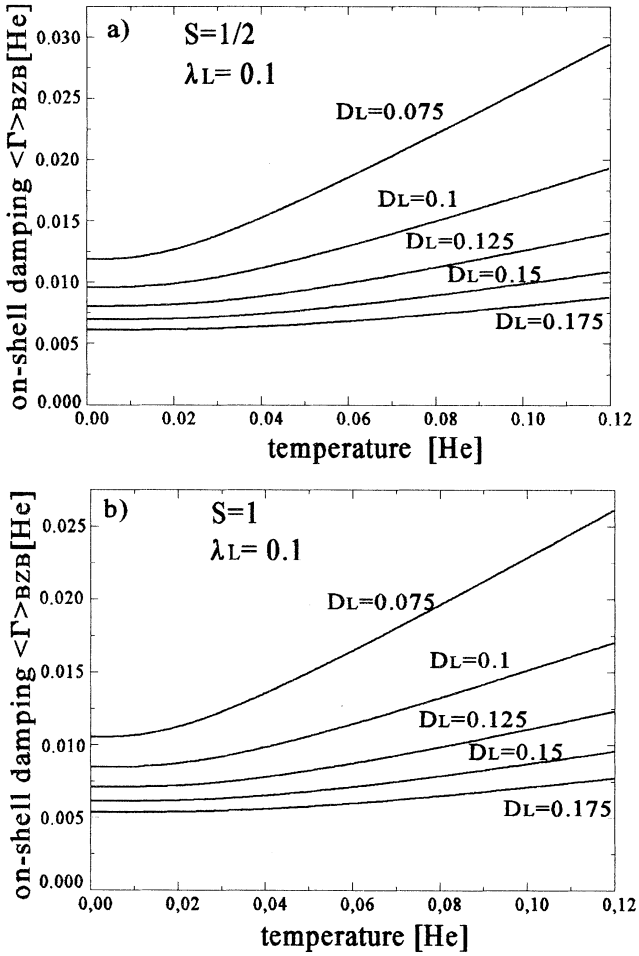

FIG. 7. Averaged damping of BZB on-shell magnons for different parameters D_L in the case of (a) spin-$\frac{1}{2}$ and (b) spin-1 with $\lambda_L = 0.1$. The damping in the case of spin-1 is slightly smaller for the same parameter D_L as in the case of spin-$\frac{1}{2}$, mainly because the in-plane renormalization constant is smaller (see text for discussion).

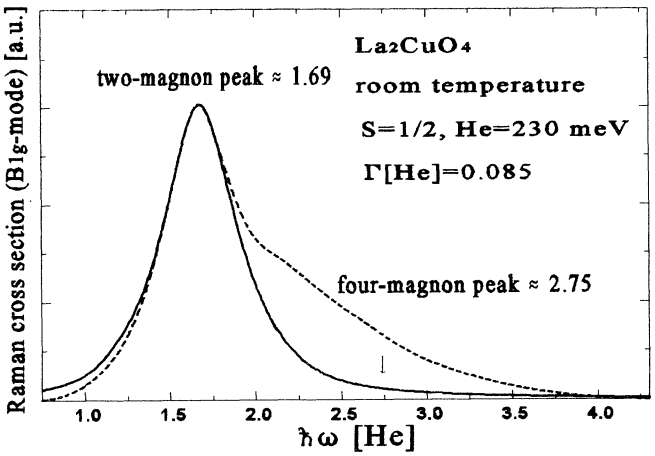

FIG. 8. The two-magnon Raman spectrum (solid line) in La_2CuO_4 ($S=1/2$) with an averaged damping of $\Gamma[H_e]=0.085$, yielding a damping in absolute units of approximately 19.5 meV, using $H_e=230$ meV, and the comparison with the experiment of Singh *et al.* (Ref. 7) (dashed line) (see text for discussion).

prates and the nickelate Pr_2NiO_4. Observe that we get a damping of 17 meV at room temperature for La_2CuO_4, if we choose a spin-phonon coupling constant of $\lambda_L=0.14$. Obviously, our qualitative model, which neglects transversally polarized and optical phonons, yields only a hint of the correct physics in the different substances, but it cannot predict the absolute values of the damping. Nevertheless, the interpretation of the spectral feature of the two-magnon Raman line in the cuprates and the nickelates is consistent in our model. Assuming the loop expansion around the spin-wave ground state holds for all spin-S, we keep only those terms which make a contribution up to order $1/S$. The $1/S^2$ contributions from the spin part of the Hamiltonian can be neglected at low temperatures and only in the regime where sound velocities are small compared to the magnon velocities does spin-phonon interaction have to be considered. That yields a significant damping of short-wavelength spin waves at zero temperature due to a possible spontaneous decay process via spin-phonon interaction and as a result a broadening of the two-magnon Raman line at low temperatures. That is the case in all the cuprates and in the nickelate Pr_2NiO_4, but not in the nickelates La_2NiO_4 and K_2NiF_4.

Considering now the experiment of Singh *et al.*[7] for the B_{1g} mode in La_2CuO_4, which was done at room temperature, we calculated the two-magnon Raman cross section, using our model with an averaged damping parameter of $\langle\Gamma\rangle_{BZB}[H_e]=0.085$. This gives a damping of approximately 19.5 meV, which lies in the same range as the damping calculated above. The reasonable agreement of our calculated two-magnon spectrum with the measured one is shown in Fig. 8. On the high-energy side, there is spectral weight missing of approximately 25%. That spectral weight results mainly from four-magnon contributions of the nearest-neighbor spin-pair excitations, neglected here, and higher contributions in the effective Raman-scattering Hamiltonian due to the resonant enhancement of the Raman cross section.[2,27] Consequently, we are not able to make a reliable prediction of its intensity. However, in order to get a rough estimate of the four-magnon peak position in the case of spin-pair excitations on neighboring sides (assuming the largest contribution to the high-energy tail comes from this process) we can add twice the two-magnon peak position of 1.69 in the case of spin-$\frac{1}{2}$ and subtract the "binding" energy of the two-magnon peak of approximately 0.626 (assuming the four-magnon "binding" energy lies in the same range as in the two-magnon case), yielding $2.75\times H_e\approx 5\times J_{\text{eff}}$, as indicated in Fig. 8. The four-magnon spectrum is now also broadened by spin-phonon interaction and there is a strong overlap between the two-magnon and the four-magnon spectrum in the case of spin-$\frac{1}{2}$. [The intensity of that four-magnon peak is at least 10% of the intensity of the two-magnon peak in the case of spin-1/2 (Ref. 25).] Applying the same technique to estimate the position of the four-magnon peak for spin-1 we obtain $\hbar\tilde{\omega}_{\text{four-magnon peak}}=2\times\hbar\tilde{\omega}_{\text{two-magnon peak}}(1.845)-\text{two-magnon}$ "binding" energy (0.313) yields 3.37 in reduced units. The latter four-magnon peak is well separated from the two-magnon peak. Consequently, there is no overlap between the two- and four-magnon spectra in the case of spin-1. In addition the intensity of the four-magnon peak in the case of spin-1 is at least a factor of 4 ($\sim 1/S^2$) smaller as in the case of spin-$\frac{1}{2}$.

Considering now the Raman experiments, performed in the two-layer system $YBa_2Cu_3O_6$,[9,11,12] the predicted damping in order to describe the linewidth of the two-magnon Raman line is approximately given by 35 meV (Refs. 11 and 38) at room temperature, being approximately twice as large as in the one-layer cuprates. We think that enhancement of the damping is produced by the magnetic coupling between the two layers[17,18] ($\alpha_{\perp 1}\approx 10^{-1}-10^{-2}$ within the notation of Ref. 18), yielding an enhancement of the coupling of displacements in the z direction onto the spins and producing a higher damping.

High-energy neutron-scattering experiments in La_2CuO_4 were done by Hayden *et al.*[14] in the direction $(0,0)-(\pi/2,\pi/2)$ (Γ-X) in square-lattice notation, showing that the one-magnon spectrum can be well fitted by a spin-wave spectrum. The damping of magnons close to the X point was measured to be smaller than 15 meV.[14,39] That is consistent with our calculations and the interpretation of the Raman-scattering experiments, because the damping at the X point is the smallest one on the BZB. It would be interesting to measure the one-magnon spectral function in the direction X-M, in order to see the increase of the damping in this direction, which would support our calculations.

V. CONCLUSION

In conclusion, we have calculated the one-magnon spectral function in the short-wavelength regime and the B_{1g} two-magnon Raman spectrum of quasi-2D antiferromagnets, generalizing the theory of Davies, Chinn, and Zeiger and Canali and Girvin,[25] taking into account the

spin-phonon interaction. As a result, we were able to show that spin-phonon interaction produces a significant damping only in the regime where sound velocities are much smaller than magnon velocities. That is due to a possible spontaneous decay process of high-energy magnons into another magnon and a phonon. This yields a consistent picture of the anomalous broad spectral feature of the two-magnon Raman line in the cuprates and the nickelate Pr_2NiO_4 being of phononic origin. This effect is absent in substances with a smaller exchange integral such as La_2NiO_4 and K_2NiF_4. Estimating, qualitatively, the four-magnon contributions caused by spin-pair excitations on neighboring sites (assuming this process makes the largest contribution to the high-energy tail in Fig. 8) we were able to explain the high-energy tail of the Raman spectrum as a consequence of the broadening of the four-magnon spectrum due to spin-phonon interaction. As a result the two-magnon line in substances with large maximum magnon energies is broadened at zero temperature. In addition, the temperature dependence of the two-magnon Raman lines, which should be nearly temperature independent in an intrinsic spin model because of the large exchange integrals, is governed by the scattering of high-energy magnons on low-energy phonons. This effect is in the two-layer system $YBa_2Cu_3O_6$ larger (at room temperature the two-magnon peak intensity is approximately 25% smaller than at low temperatures) than in the one-layer cuprates (at room temperature the two-magnon peak intensity is approximately 10% smaller than at low temperatures) due to the magnetic coupling between the two layers. This yields an enhanced coupling of displacements in the out-of-plane direction onto the spins and gives as a result a larger damping due to spin-phonon interaction in two-layer systems. The temperature dependence of the Raman lines in 2D antiferromagnets with smaller maximum magnon energies such as, e.g., the nickelate La_2NiO_4, is mainly due to decay processes of high-energy magnon via spin-spin interaction and spin-phonon interaction can be neglected in such substances. Consequently the Raman line is very narrow at low temperatures and the rapid decrease of its peak intensity and the broadening of the Raman cross section (at room temperature the two-magnon peak intensity is approximately 50% smaller than at low temperatures) is due to the increase of the damping of high-energy magnons due to spin-spin interaction with temperature.

ACKNOWLEDGMENTS

The author acknowledges useful discussions on nonlinear optics with Dr. U. Becker and Professor Dr. A. Holz, and Dr. G. Aeppli for stimulating correspondence.

APPENDIX: THE SPIN-PHONON VERTICES IN RHA

The spin-phonon vertices in RHA, used in (23) in the main text, are given by

$$g_{\alpha^+\alpha}(\mathbf{q},\mathbf{k}_1,\mathbf{k}_2,j)=\frac{1}{\sqrt{m(\mathbf{q})}}\{\bar{\Delta}(\mathbf{q},j,\mathbf{q})u_{k_1}u_{k_2}+\bar{\Delta}(\mathbf{q},j,\mathbf{k}_1-\mathbf{k}_2)v_{k_1}v_{k_2}+[\bar{\Delta}(\mathbf{q},j,\mathbf{k}_2)-\bar{\Delta}(\mathbf{q},j,\mathbf{k}_2+\mathbf{q})]u_{k_1}v_{k_2}$$
$$-[\bar{\Delta}(\mathbf{q},j,\mathbf{k}_1)-\bar{\Delta}(\mathbf{q},j,\mathbf{k}_1-\mathbf{q})]u_{k_2}v_{k_1}\}\ , \tag{A1}$$

$$g_{\beta^+\beta}(\mathbf{q},\mathbf{k}_1,\mathbf{k}_2,j)=\frac{1}{\sqrt{m(\mathbf{q})}}\{\bar{\Delta}(\mathbf{q},j,\mathbf{q})v_{k_1}v_{k_2}+\bar{\Delta}(\mathbf{q},j,\mathbf{k}_1-\mathbf{k}_2)u_{k_1}u_{k_2}+[\bar{\Delta}(\mathbf{q},j,\mathbf{k}_2)-\bar{\Delta}(\mathbf{q},j,\mathbf{k}_2+\mathbf{q})]v_{k_1}u_{k_2}$$
$$-[\bar{\Delta}(\mathbf{q},j,\mathbf{k}_1)-\bar{\Delta}(\mathbf{q},j,\mathbf{k}_1-\mathbf{q})]v_{k_2}u_{k_1}\}\ , \tag{A2}$$

$$g_{\alpha^+\beta^+}(\mathbf{q},\mathbf{k}_1,\mathbf{k}_2,j)=\frac{-1}{\sqrt{m(\mathbf{q})}}\{\bar{\Delta}(\mathbf{q},j,\mathbf{q})v_{k_1}u_{k_2}+\bar{\Delta}(\mathbf{q},j,\mathbf{k}_1-\mathbf{k}_2)u_{k_1}v_{k_2}+[\bar{\Delta}(\mathbf{q},j,\mathbf{k}_2)-\bar{\Delta}(\mathbf{q},j,\mathbf{k}_2+\mathbf{q})]v_{k_1}v_{k_2}$$
$$-[\bar{\Delta}(\mathbf{q},j,\mathbf{k}_1)-\bar{\Delta}(\mathbf{q},j,\mathbf{k}_1-\mathbf{q})]u_{k_2}u_{k_1}\}\ , \tag{A3}$$

$$g_{\alpha\beta}(\mathbf{q},\mathbf{k}_1,\mathbf{k}_2,j)=\frac{-1}{\sqrt{m(\mathbf{q})}}\{\bar{\Delta}(\mathbf{q},j,\mathbf{q})u_{k_1}v_{k_2}+\bar{\Delta}(\mathbf{q},j,\mathbf{k}_1-\mathbf{k}_2)v_{k_1}u_{k_2}+[\bar{\Delta}(\mathbf{q},j,\mathbf{k}_2)-\bar{\Delta}(\mathbf{q},j,\mathbf{k}_2+\mathbf{q})]u_{k_1}u_{k_2}$$
$$-[\bar{\Delta}(\mathbf{q},j,\mathbf{k}_1)-\bar{\Delta}(\mathbf{q},j,\mathbf{k}_1-\mathbf{q})]v_{k_2}v_{k_1}\}\ , \tag{A4}$$

implying momentum conservation $\mathbf{k}_1=\mathbf{k}_2+\mathbf{q}+\mathbf{G}$, where $\mathbf{G}$ is a reciprocal-lattice vector of the magnetic lattice. Upon interchange of wave vectors we get the symmetry properties

$$\begin{aligned}
&g_{\alpha^+\alpha}(\mathbf{q},\mathbf{k}_1,\mathbf{k}_2,j)=-g_{\alpha^+\alpha}(-\mathbf{q},\mathbf{k}_2,\mathbf{k}_1,j)\ ,\\
&g_{\beta^+\beta}(\mathbf{q},\mathbf{k}_1,\mathbf{k}_2,j)=-g_{\beta^+\beta}(-\mathbf{q},\mathbf{k}_2,\mathbf{k}_1,j)\ ,\\
&g_{\alpha^+\beta^+}(\mathbf{q},\mathbf{k}_1,\mathbf{k}_2,j)=-g_{\alpha^+\beta^+}(-\mathbf{q},\mathbf{k}_2,\mathbf{k}_1,j)\ ,\\
&g_{\alpha\beta}(\mathbf{q},\mathbf{k}_1,\mathbf{k}_2,j)=-g_{\alpha\beta}(-\mathbf{q},\mathbf{k}_2,\mathbf{k}_1,j)\ ,\\
&g_{\alpha^+\beta^+}(\mathbf{q},\mathbf{k}_1,\mathbf{k}_2,j)=-g_{\alpha\beta}(-\mathbf{q},\mathbf{k}_2,\mathbf{k}_1,j)\ ,
\end{aligned} \tag{A5}$$

where we used the following relation for the phonon eigenvectors:

$$\mathbf{e}(\mathbf{q},j)=\mathbf{e}(-\mathbf{q},j)\ . \tag{A6}$$

In addition, considering the momentum conservation, we obtain the equalities

$$\begin{aligned}
&g_{\alpha^+\alpha}(\mathbf{q},\mathbf{k}_1,\mathbf{k}_2,j)=\pm g_{\beta^+\beta}(\mathbf{q},\mathbf{k}_1,\mathbf{k}_2,j)\ ,\\
&g_{\alpha^+\beta^+}(\mathbf{q},\mathbf{k}_1,\mathbf{k}_2,j)=\pm g_{\alpha\beta}(\mathbf{q},\mathbf{k}_1,\mathbf{k}_2,j)\ .
\end{aligned} \tag{A7}$$

The upper sign refers to umklapp processes, where the reciprocal-lattice vector is an element of the mechanical lattice (nuclear Bragg peaks), and the lower sign in (A7) refers to umklapp processes, where the reciprocal-lattice vector is only element of the magnetic lattice (magnetic Bragg peaks).

*Present address: Institut für Neue Materialieu, im Stadtwald 66123 Saarbrücken, Germany.

[1]S. R. Chinn, H. J. Zeiger, and J. R. O'Connor, Phys. Rev. B **3**, 1709 (1970).
[2]B. S. Shastry and B. I. Shraiman, Phys. Rev. Lett. **65**, 1068 (1990).
[3]J. B. Parkinson, J. Phys. C **2**, 2012 (1969).
[4]R. W. Davies, S. R. Chinn, and H. J. Zeiger, Phys. Rev. B **4**, 992 (1971).
[5]P. Fleury and R. Loudon, Phys. Rev. **166**, 514 (1968).
[6]R. J. Elliott and M. F. Thorpe, J. Phys. C **2**, 1630 (1969).
[7]P. R. P. Singh, P. A. Fleury, K. B. Lyons, and P. E. Sulewski, Phys. Rev. Lett. **62**, 2736 (1989).
[8]P. E. Sulewski, P. A. Fleury, and K. B. Lyons, Phys. Rev. B **41**, 225 (1990).
[9]S. Sugai *et al.*, Phys. Rev. B **42**, 1045 (1990).
[10]S. Sugai, T. Kobayashi, and J. Akimitsu, Phys. Rev. B **40**, 2686 (1989).
[11]P. Knoll, C. Thompsen, M. Cardona, and P. Murugaraj, Phys. Rev. B **42**, 4842 (1990).
[12]K. B. Lyons, P. A. Fleury, L. F. Schneemeyer, and J. V. Waszczak, Phys. Rev. Lett. **60**, 732 (1988).
[13]A. de Andrés, J. L. Martinez, and P. Odier, Phys. Rev. B **45**, 12 821 (1992).
[14]G. Aeppli and D. J. Buttrey, Phys. Rev. Lett. **61**, 203 (1988); G. Aepply *et al.*, *ibid.* **62**, 2052 (1989); S. M. Hayden *et al.*, *ibid.* **67**, 3622 (1991).
[15]B. Keimer *et al.*, Phys. Rev. B **45**, 7430 (1992).
[16]B. Keimer *et al.*, Phys. Rev. B **46**, 14 034 (1992).
[17]J. Rossat-Mignod *et al.*, Physica B **163**, 4 (1990).
[18]J. M. Tranquada *et al.*, Phys. Rev. B **40**, 4503 (1989).
[19]S. Chakravarty, B. I. Halperin, and D. R. Nelson, Phys. Rev. B **39**, 2344 (1989).
[20]S. Tyč and B. I. Halperin, Phys. Rev. B **42**, 2096 (1990).
[21]P. Kopietz, Phys. Rev. B **41**, 9228 (1990).
[22]P. Kopietz, Phys. Rev. Lett. **68**, 3480 (1992).
[23]G. E. Castilla and S. Chakravarty, Phys. Rev. B **43**, 13 687 (1991).
[24]E. Monousakis, Rev. Mod. Phys. **63**, 1 (1991).
[25]C. M. Canali and S. M. Girvin, Phys. Rev. B **45**, 7127 (1992).
[26]D. U. Sänger, Phys. Rev. B **49**, 12 176 (1994).
[27]In the framework of the effective one-band Hubbard model, i.e., U is replaced by the charge-transfer gap E_{CTG} (Refs. 29 and 30), the frequencies of the incident light used in the experiments (the main laser lines of an Argon-ion laser used in experiments have energies of $\hbar\omega = 2.41$, 2.54 or 2.7 eV) are in resonance in the sense that the energy of the incident light is close to the charge-transfer gap (≈ 1.7 eV). As a result, the B_{1g} Raman spectrum is resonantly enhanced due to excitations into states being located close to the charge-transfer gap. Furthermore, there exists also a finite Raman cross section also in the A_{1g} and B_{2g} symmetry and one obtains higher contributions in the effective Raman-scattering Hamiltonian in B_{1g} geometry, which produce at least partially the high-energy tail in the B_{1g} mode. As a further consequence, spin-pair excitations cannot be measured by the Raman process in the highly doped substances, because absorption decreases for the laser frequencies, usually used in the experiments, with increasing doping, yielding a weakening of the resonant enhancements with doping. On the other hand, the line shape of the Raman spectrum remains unchanged with doping up to $x \sim 0.5$ in $YBa_2Cu_3O_{6+x}$ (Ref. 28), showing that the spin dynamics in the short-wavelength limit is unaffected by doping. This stands in strong contradiction to calculations of the one-magnon spectral function, postulating mobile holes in the 2D Heisenberg antiferromagnet (Refs. 40), causing a strong softening of the magnon dispersion and an increased damping of short-wavelength magnons.
[28]S. L. Cooper *et al.*, Phys. Rev. B **47**, 8233 (1993); D. Reznik *et al.*, *ibid.* **48**, 7624 (1993).
[29]A. Kampf, Phys. Rep. **249**, 219 (1994).
[30]F. C. Zhang and T. M. Rice, Phys. Rev. B **37**, 3759 (1988).
[31]M. G. Cottam, J. Phys. C **7**, 2901 (1974).
[32]F. J. Dyson, Phys. Rev. **102**, 1217 (1956).
[33]S. V. Maleev, Zh. Eksp. Theor. Fiz. **30**, 1010 (1957) [Sov. Phys. JETP **64**, 654 (1958)].
[34]A. B. Harris, D. Kumar, B. I. Halperin, and P. C. Hohenberg, Phys. Rev. B **3**, 961 (1971).
[35]P. C. Hohenberg, Phys. Rev. **158**, 383 (1967).
[36]N. D. Mermin and H. Wagner, Phys. Rev. Lett. **17**, 1133 (1966).
[37]S. W. Lovesey, *Condensed Matter Physics Dynamic Correlations* (Benjamin/Cummings, Reading, MA, 1980).
[38]W. H. Weber and G. W. Ford, Phys. Rev. B **40**, 6890 (1989).
[39]G. Aeppli (private communication).
[40]I. R. Pimentel and R. Orbach, Phys. Rev. B **46**, 2920 (1992); J. Igarashi and P. Fulde, *ibid.* **45**, 10 419 (1992); G. Khaliullin and P. Horsch, *ibid.* **47**, 463 (1993); G. Krier and G. Meissner, Ann. Phys. (Leipzig) **2**, 738 (1993).